MATHEMATICAL SIMULATION OF INFILTRATING WATERSHEDS

By

ROGER E. SMITH and DAVID A. WOOLHISER

January 1971

HYDROLOGY PAPERS
COLORADO STATE UNIVERSITY
Fort Collins, Colorado

47

MATHEMATICAL SIMULATION OF INFILTRATING WATERSHEDS

by

Roger E. Smith

and

David A. Woolhiser

HYDROLOGY PAPERS

COLORADO STATE UNIVERSITY

FORT COLLINS, COLORADO 80521

January 1971 No. 47

ACKNOWLEDGMENTS

This paper is based upon the Ph.D. dissertation "Mathematical Simulation of Infiltrating Watersheds" by Roger E. Smith. The work was supported by the Northern Plains Branch, Agricultural Research Service, USDA, in cooperation with the Colorado State University Agricultural Experiment Station. The Agricultural Engineering Department provided the facilities of the Porous Media Laboratory and some of the scintillation counting equipment used in this study. D. B. McWhorter provided part of the experimental data on the Poudre fine sand.

Dr. E. A. Breitenbach made many helpful suggestions on numerical methods. The help and advice of Dr. M. E. Holland, Dr. R. E. Niemann, Dr. E. V. Richardson and Dr. J. C. Ward is also sincerely appreciated.

TABLE OF CONTENTS

LIST OF FIGURES AND TABLES

ABSTRACT

The partial differential equation for vertical, one-phase, unsaturated flow of water in soils is used as a mathematical model governing infiltration. A nonlinear Crank-Nicolson implicit finite-difference scheme is used to obtain solutions to this equation for realistic initial and upper boundary conditions. The kinematic wave approximation to the equations of unsteady overland flow on cascaded planes is used for the mathematical model of surface runoff. The difference equations of infiltration and overland flow are combined into a model for a simple watershed, employing computational logic so that boundary conditions match at the soil surface. The mathematical model is tested by comparison with data from a laboratory soil flume and with data from a small experimental watershed.

MATHEMATICAL SIMULATION OF INFILTRATING WATERSHEDS*

by

Roger E. Smith** and David A. Woolhiser***

CHAPTER I

INTRODUCTION

The Watershed. Starting from a point P on a stream, of any size, one may define a topographic unit from which the stream gathers its water. Moving laterally from this point on the stream, one may trace a line which will describe the outermost point from which water will move into a tributary of the stream above P. All points outside this line will drain either downstream of point P, or into a different stream. The area enclosed by this topographic line is called a watershed. It may also be called a drainage basin, or a catchment. The Continental Divide, on a grand scale, is the line where all watersheds of North America that flow into the Atlantic meet those flowing into the Pacific.

As one moves the point P upstream, the watershed corresponding to P becomes successively smaller. At the point where the defined stream disappears, the contributing area may be called a watershed element, or an overland flow area. The lateral boundaries of this unit are streamlines of surface water flow, and the upper boundary is a topographic divide. Still, we may refer to such an area as a watershed.

Considering the surface contribution only, all large watersheds are made up of a complex arrangement of small overland flow units and stream channels. By reducing the watershed to its simplest form, the overland flow area, we have a natural system with comparatively simple boundary conditions. The major variables involved in this system are rainfall, evapotranspiration, and groundwater flow. The watershed system may vary in terms of moisture stored in both the unsaturated and saturated soil regions, in the state of vegetative cover, the surface conditions such as occur on plowed land, and changes due to seasonal effects. Assuming that the groundwater surface reflects the topography, there is negligible flow through the vertical surfaces defining the lateral and upstream boundaries of the system. Rainfall enters the system as lateral inflow and water emerges from the downstream boundary either as subsurface flow, or as surface runoff.

The process by which rainfall enters the soil through the surface is called infiltration. Many factors affect infiltration by changing the soil structure, such as compaction of the soil by man and animals, subsurface modifications by insects, changing root patterns, and seasonal freeze and thaw. For any given state of the soil structure, the infiltration rate is largely governed by the amount and distribution of moisture in the soil. This study will assume the soil structure to be constant and will consider infiltration rate to be a function of moisture content and distribution.

Given this restriction, that the soil in the elementary watershed is physically constant, one may treat the watershed as a system that will receive rainfall, accept some of it as soil moisture, eliminate some as overland flow, and divide the accepted water among groundwater storage, subsurface flow, and evapotranspiration. The problem treated in this work is the description of the process whereby surface runoff is produced from rainfall on the watershed. For this purpose the system will be studied by means of a model.

Strategy of Models. Models are useful tools in the study of natural processes. All natural processes are more or less complex. The most complex ones, such as next week's weather, involve so many inputs and variables that either they cannot be enumerated, or all variables cannot be measured. For this case, a statistical model is most often used to describe the output (or a selected variable) in terms of the statistical properties of the historical data concerning the process. One may correlate all conceptually related, measured variables with the variable of interest, by statistical methods, to obtain a statistical regression model for the process. Where the relationship between a number of variables adequately describes the "output" variable, the relation so developed from observation is called an empirical model.

When the process is sufficiently understood on the basis of physical laws or physical theory, then the process may be described by a theoretical model. If the process is not understood in terms of theory, but can be isolated, a physical model, which is

---

* Contribution from the Colorado Agricultural Experiment Station and the Northern Plains Branch, Soil and Water Conservation Research Division, Agricultural Research Service, USDA, Fort Collins, Colorado.

** Research Hydraulic Engineer, USDA, Tucson, Arizona (formerly Graduate Research Assistant, Colorado State University.)

***Research Hydraulic Engineer, USDA, Fort Collins, Colorado.

actually a material representation, may be used. A laboratory flume is a material model.

Models of any of these forms are means by which the complex natural processes may be isolated and studied, to better understand their function. The description given above of the watershed as a system is a conceptual model in itself. If the model is physically based, then it may also be used to predict the function of the system for conditions not observed in historical data, or to show how the system will function if the system properties are changed.

Objective. The purpose of this study is to (a) develop a mathematical model for an elementary watershed, combining physically derived differential equations for overland flow and soil infiltration from a rainfall source; (b) obtain numerical solutions to these equations; and (c) investigate the applicability of this model by comparison with the performance of a laboratory-scale prototype watershed, and data from a field plot watershed.

CHAPTER II

EVOLUTION OF MATHEMATICAL MODELS OF INFILTRATION

Algebraic Infiltration Equations

The first mathematical descriptions of infiltration were empirical formulas developed to describe the results of infiltrometer tests. The earliest infiltrometer was basically a ring driven into the ground, and infiltration rate was measured as the rate of application needed to maintain a constant level of ponded water within the ring. This method has now been largely replaced by a sprinkling application, using a larger bounded area. In either case, the resulting empirical equations describe a rate of infiltration decreasing from an initial maximum rate to a final minimum rate. The most common of these have been discussed by Amorocho [1967] and Philip [1957].

A few of these formulas will be presented as examples. The following algebraic equation is a popular one developed by Horton [1940]:

$$f = f_e + (f_o - f_e)e^{-kt} \qquad (2.1)$$

Here f = infiltration rate at time t. f_e and f_o are infiltration rates at $t = \infty$ and $t = 0$, respectively. The constant k is a best fit parameter, and has little or no physical significance.

A somewhat more general formula was proposed by Holtan [1961] to describe infiltration and redistribution:

$$f = f_e + a(S - F)^n \quad ; \qquad (2.2)$$

f_e, a, and n are experimentally determined constants. $S-F$ represents the hypothetical available soil moisture storage where $F(t) = \int_o^t f(s)ds$. The maximum value of S is the soil porosity above some impeding layer. This is a nonlinear storage type of time-dependent formula, fitted empirically to infiltrometer or watershed data. In a later paper [Holtan, et.al., 1967], Holtan expands this formula to make a precipitation routing model, where S is subdivided into a portion called capillary storage (AWC), and another termed free-water storage (G). AWC is filled by f, and when F becomes $>$ AWC, water goes into free-water storage and can drain downward at a rate not exceeding f_e. Another empirical model describes evapotranspiration from storage AWC between rains. This is a commendable algebraic model in that it does attempt to account for recovery of infiltration capacity.

Perhaps the most complex precipitation routing model to date is one developed by Crawford and Linsley [1966], called the Stanford Watershed Model. The model fits parameters from historical data for processes of infiltration, evaporation, surface runoff and streamflow for large watersheds. Although it is essentially a "lumped" model, it does presume a uniform distribution of properties, including infiltration rates, over the watershed. Again, the fitted parameters have doubtful physical significance, if any.

These few examples should be sufficient to demonstrate the limitations of algebraic-empirical infiltration models. Firstly, many of them consider only infiltration from a ponded surface, which is a poor model for rainfall. Even when sprinklers are used, the data are good for only that rate of application, and assumptions must be made for other rainfall rates. Rainfall seldom falls at a given rate for very long. Secondly, as pointed out, the parameters developed have little or no physical meaning, in that they cannot be determined or estimated from knowledge of the soil, surface cover, etc. Finally, most equations cannot account for changes in initial soil water content and therefore cannot accurately predict the time of beginning of runoff and are not applicable for intermittent rainfall. The Stanford model and the Holtan equation are exceptions to this statement.

Infiltration Rates from Soil Water Flow Equations

Progress in knowledge of the flow of water in soils, along with the mathematical tools for its description, has led to another approach to describing infiltration. Let us presume that we can determine the appropriate hydraulic properties of a given soil, and write equations that describe movement of water through the soil. Then if we supply rainfall at a given rate at the surface, the infiltration of water into the soil is a dependent boundary condition with a rate determined at a given time by the state of the soil itself.

Water Flow Equations. The equations appropriate for this case are those of two-phase fluid flow in porous media. The two fluid phases are air and water, and soil is the porous medium. Although equations may be written for three-dimensional flow, only vertical flow of each fluid will be considered here. The vertical dimension Z will be measured downward from the soil surface; h will represent distance to a point above an arbitrary datum, measured positive upward. Subscript a refers to air, and subscript w refers to water. Thus for a point within the soil, we have the following equations:

A. Continuity equations

air: $$\frac{\partial}{\partial Z}\rho_a q_a + \frac{\partial}{\partial t}(\phi S_a \rho_a) = 0 \qquad (2.3)$$

water: $$\frac{\partial}{\partial Z} q_w + \frac{\partial}{\partial t}(\phi S_w) = 0 \qquad (2.4)$$

B. Darcy equations for flow

air: $$q_a = \frac{-kk_{ra}}{\mu_a} \frac{\partial}{\partial Z}(p_a + \rho_a g h) \qquad (2.5)$$

water: $$q_w = \frac{-kk_{rw}}{\mu_w} \frac{\partial}{\partial Z}(p_w + \rho_w g h) \qquad (2.6)$$

C. Fluid conservation

$$S_w + S_a = 1 \qquad (2.7)$$

D. Definition of capillary pressure

$$p_c = p_a - p_w \qquad (2.8)$$

In which

ρ = density	ML^{-3}
q = velocity (volume flux)	LT^{-1}
ϕ = porosity	
S = volumetric saturation - the ratio of the volume of wetting fluid to the volume of the interconnected pore space in a bulk element of the medium.	
g = gravitational acceleration	LT^{-2}
k = permeability	L^2
k_r = relative permeability or relative conductivity	
μ = dynamic viscosity	$ML^{-1}T^{-1}$
p = pressure	$ML^{-1}T^{-2}$
h = elevation potential	L
p_c = capillary pressure	$ML^{-1}T^{-2}$

We can immediately combine the Darcy equations with the continuity equations to form the following basic equations:

air: $$\frac{\partial}{\partial Z}\left[-\rho_a \frac{kk_{ra}}{\mu_a} \frac{\partial}{\partial Z}(p_a + \rho_a g h)\right] + \frac{\partial}{\partial t}(\phi S_a \rho_a) = 0 \qquad (2.9)$$

water: $$\frac{\partial}{\partial Z}\left[\frac{-kk_{rw}}{\mu_w} \frac{\partial}{\partial Z}(p_w + \rho_w g h)\right] + \frac{\partial}{\partial t}(\phi S_w) = 0 \; . \qquad (2.10)$$

To solve this system of equations, it is necessary to utilize equation (2.8) to replace either p_a or p_w by the expression for capillary pressure. S_a, S_w, k_{ra} and k_{rw} are all functions of p_c, and the equations then become equations in p_a and p_c or p_w and p_c. This may be accomplished as follows:

From equation (2.3), $$\frac{\partial p_c}{\partial Z} = \frac{\partial p_a}{\partial Z} - \frac{\partial p_w}{\partial Z}$$

or $$\frac{\partial p_a}{\partial Z} = \frac{\partial p_c}{\partial Z} + \frac{\partial p_w}{\partial Z} \qquad (2.11)$$

Thus equation (2.9) may be rewritten

$$\frac{\partial}{\partial Z}\left\{-\rho_a \frac{kk_{ra}}{\mu_a}\left[\frac{\partial p_c}{\partial Z} + \frac{\partial p_w}{\partial Z} + g\frac{\partial(\rho_a h)}{\partial Z}\right]\right\} + S_a \frac{\partial}{\partial t}(\phi \rho_a) + \phi \rho_a \frac{\partial S_a}{\partial t} = 0 \qquad (2.12)$$

from equation (2.7)

$$\frac{\partial S_a}{\partial t} + \frac{\partial S_w}{\partial t} = 0 \qquad (2.13)$$

and using the fact that $\frac{\partial}{\partial Z}(\rho_w g h) = -\rho_w g$, equation (2.10) may be rewritten

$$\frac{\partial}{\partial Z}\left[-\frac{kk_{rw}}{\mu_w}\left(\frac{\partial p_w}{\partial Z} - \rho_w g\right)\right] + S_w \frac{\partial \phi}{\partial t} + \phi \frac{\partial S_w}{\partial t} = 0 \; . \qquad (2.14)$$

Now using (2.13), equations (2.14) and (2.12) may be combined thus:

$$\frac{\partial}{\partial Z}\left[-\rho_a \frac{kk_{ra}}{\mu_a}\left(\frac{\partial p_c}{\partial Z} + \frac{\partial p_w}{\partial Z} + g\frac{\partial}{\partial Z}(\rho_a h)\right)\right] + (1 - S_w)\frac{\partial}{\partial t}(\phi \rho_a) + \rho_a \frac{\partial}{\partial Z}\left[\frac{-kk_{ra}}{\mu_w}\left(\frac{\partial p_w}{\partial Z} - \rho_w g\right)\right] + S_w \rho_a \frac{\partial \phi}{\partial t} = 0 \qquad (2.15)$$

to eliminate specific reference to p_a.

Thus equations (2.14) and (2.15) form a pair of simultaneous, nonlinear, parabolic partial differential equations in p_w, p_c, and t.

In a great many cases in soil physics, these equations are simplified considerably by the assumption that air moves under negligible pressure gradients, i.e., μ_a is very small, and p_a is practically constant. In this case, equation (2.10) may be used to describe soil moisture movement, and may be simplified by noting that if $p_a = 0$, $p_w = -p_c$, so that

$$\frac{\partial}{\partial t}(\phi S_w) = \frac{\partial}{\partial Z}\left[\frac{k k_{rw} \gamma_w}{\mu_w}\left(\frac{\partial \psi}{\partial Z} - 1\right)\right]$$

where $\psi = p_w/\gamma_w$ is capillary potential, and γ_w is the specific weight of water. $\frac{k_w \gamma_w}{\mu_w}$ is the conductivity K of the medium to water, in units of L/T, and we may write

$$\frac{\partial}{\partial t}(\phi S_w) = K\frac{\partial}{\partial Z}\left(k_r \frac{\partial \psi}{\partial Z}\right) - K\frac{\partial k_r}{\partial Z} \quad . \qquad (2.16)$$

This commonly used equation is often referred to as "Richards equation" after L. A. Richards [1931]. Its solution depends on knowing the functional relationships among ψ, S_w, and k_r, for the particular soil in question.

Equation (2.16) may be applied to many types of unsaturated flow problems, depending on the particular boundary conditions chosen. For rainfall infiltration, for example, the upper boundary conditions are:

a) $t_o < t < t_p$: $f(0,t)$ = rainfall rate

where t_p = time at which $\theta(0,t) = \theta$ saturated,

or $\psi(0,t) = 0$; $\theta = \phi S_w$; and f is the infiltration rate.

b) $t > t_p$, $\psi(0,t) = 0$.

The initial conditions may be any physically realizable array of pressures

$$\psi(Z,0) = \psi \text{ initial}, \quad 0 < Z < L \quad .$$

The lower boundary conditions may be a water table at some depth L, such that

$$\psi(L,t) = 0, \quad 0 < t < \infty \quad .$$

The solution surface for such a problem is illustrated in Fig. 2.1, showing θ as a function of Z,t. The equation is actually solved in terms of ψ, although the variable θ is often of greater interest. This is due to the fact that, for transformation to a θ based equation, the term $\partial\psi/\partial\theta$ appears, which becomes large without limit near saturation (see Fig. 2.2). Richard's equation was developed in somewhat different forms by various other investigators, including Gardner and Widtsoe [1921], and Childs and Collis-George [1950] who were among the first to recognize that (Kk_r) is a nonlinear, saturation-dependent variable. The history of this equation is well summarized by Gardner [1967].

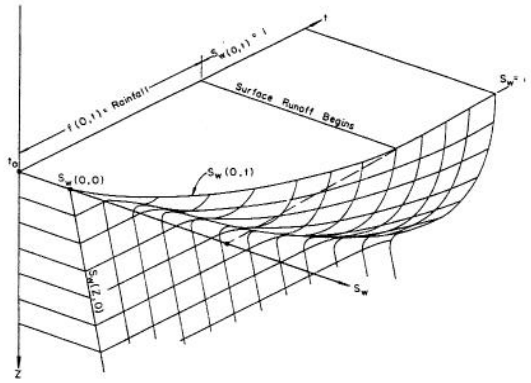

Fig. 2.1. Solution surface in (S_w, z, t) for equation (2.16).

Important Assumptions. Infiltration is a dependent boundary condition of the soil water movement equations, and this mathematical model cannot describe infiltration accurately if it cannot model soil water movement accurately. It is important that the assumptions behind this mathematical model (equation (2.16)) be recognized.

(a) It is a one-dimensional model which assumes the soil surface to be a plane, although similar two- and three-dimensional equations can easily be written

(b) Capillary suction ψ and unsaturated conductivity k_r are unique, time invarient functions of saturation θ. This model therefore neglects seasonal variation, effects of raindrop impact, and other structural changes.

(c) Darcy's law is valid for unsaturated flow, provided assumption (b) holds.

(d) The relations referred to in (b), which can be evaluated in steady state soil tests, are true as well for a dynamic or unsteady flow situation.

It is reasonable to accept a one-dimensional model for rainfall entering soil, where variations of conditions are relatively uniform over a substantial area, and the water table is sufficiently deep. For a given soil structure, assumption (b) is supported by experimental evidence. Verification of assumptions (c) and (d) is more difficult, yet no known evidence exists to show that these assumptions are far in error.

Importance of Hydraulic Properties of the Soil. Equation (2.16), without severely simplifying assumptions, cannot be solved analytically, and it is commonly solved by numerical methods. The solution depends on a knowledge of two basic hydraulic relationships for the soil involved. These describe the relationships among θ, ψ, and k_r, expressed as $k_r(\theta)$ and $\psi(\theta)$, or $k_r(\psi)$ and $\theta(\psi)$.

It has been known for some time that during moisture uptake each soil exhibits a unique relation between θ and ψ [16]. Unfortunately, this curve is not generally determined as a basic soil property. Several investigators have attempted to describe this relation by empirical equations, but the parameters involved generally have no relation to physical, measurable soil properties. This relationship is complicated by the fact that soils exhibit a varying amount of hysteresis between wetting (imbibition) and drying (desaturation) processes. If only one or the other process is concerned, this hysteresis can be neglected. Partly due to the experimental difficulties involved in determining imbibition curves, many more analyses of desaturation curves for soils are available in literature.

White [1968] presented a quite complex empirical equation for describing the desaturation curves, along with some physical justification for the forms of the equations. The equation of Brooks and Corey [1964] is much simpler, but neglects the region near saturation, which is very important in infiltration studies (see Chapter V).

Rubin [1966] developed an empirical equation for a particular sand, using nine parameters to describe both wetting and drying curves. Other writers who have proposed empirical formulations include Rubin and Steinhardt [1963], King [1964] and Phuc [1969]. Brutsaert [1966] developed a simplified surface tension model to transform pore radius distribution to a capillary suction relation. With the present state of knowledge of soil physics, this θ-ψ relation should be considered a basic soil property to be determined for each soil by experiment.

The relation of conductivity to moisture content of soils (or to capillary suction) has received considerable attention from soil physicists. Childs and Collis-George [op.cit.], in an attempt to derive a theoretical equation, proposed a relation describing saturated conductivity based on the theoretical distribution and interaction of pore sizes. Following this type of statistical analysis of pore size distributions, Marshall [1958] derived an expression for "effective" pore size and, like Brutsaert [op.cit.], related this to a distribution of ψ. To describe the unsaturated conductivity of a soil as a function of S_e, Irmay [1954] derived the relation

$$k_r = S_e^{\varepsilon} \tag{2.17}$$

where ε is 3.

Brooks and Corey [op.cit.], on the basis of certain theoretical assumptions and extensive experimental data, have generalized this relationship to make ε a parameter, related to the parameter λ in the empirical relation between capillary pressure and saturation:

$$S_e = \left(\frac{p_b}{\psi}\right)^{\lambda} \quad \text{for} \quad \psi > p_b \tag{2.18}$$

and

$$\varepsilon = \frac{2 + 3\lambda}{\lambda} \,. \tag{2.19}$$

Several investigators have used the product $k_r(\theta)\frac{\partial\psi}{\partial\theta}$, known as the diffusivity, $D(\theta)$, and have derived empirical relations for this rather than k_r (Jackson, [1963]). Example curves for the above soil relationships are shown in Fig. 2.2.

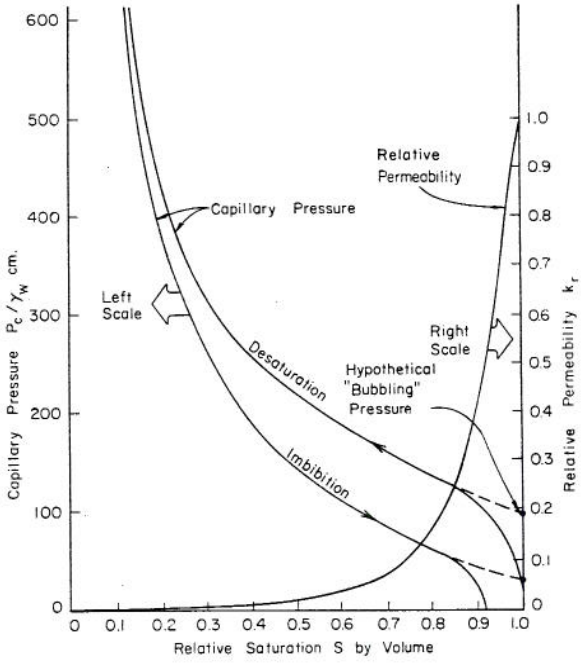

Fig. 2.2. Typical relationships between unsaturated hydraulic properties of soils.

The complexity of the physics involved in these relationships should be emphasized. Soils that may be quite similar in terms of agricultural properties may be quite different as porous media. Factors such as concentration of ions, chemical interaction of water with the clay fraction of the soil and nonhomogeneity complicate the picture in the field situation. Swelling soils also change the simple relationships (See Chapter IV).

Melrose [1965] has studied the thermodynamics and physics involved in some detail. Paulovassilis [1962]

and Philip [1964] have published mathematical models that attempt to describe hysteresis in particular soils. Melrose [op.cit] and Miller and Miller [1955] have given very plausible microscopic explanations for the cause of hysteresis. These and other studies can only scratch the surface of the complex physical system involved.

Numerical Solutions to Soil Water Equations

The equation for horizontal, unsaturated flow in porous media, neglecting air pressure, is of the same form as equation (2.16) with the rightmost term removed. Klute [1952] solved this equation numerically, using a transformation of variables and a constant upper boundary saturation. Later, Philip [1957] showed a method for applying similar solution techniques to the vertical case, using a series of successive approximations. With a hand calculator, this method was quite laborious. Again, a given saturation at the surface for $t > 0$ was used as the upper boundary condition.

With the development of high-speed digital computers, the method of finite differences was applied to this equation, and researchers have developed methods to solve equation (2.16) for boundary conditions better approximating real situations for a variety of applications. Several of the most important contributors to solution techniques for the problem of vertical downward flow of moisture from surface input and the major features of their numerical methods are listed in Table 2.1. All of the more recent investigators have employed finite difference techniques, which essentially consist of rewriting equation (2.16) as a finite difference equation rather than a partial differential equation, and proceeding numerically with small increments of time, solving for the pressures at each point in the vertical. Most of the authors employed a linearized form of the equation--i.e., the coefficients such as $k_r(\psi,t)$, instead of being variables as is $\psi(t)$, are taken as constants over a time increment, using values of ψ at $t - \Delta t$. This creates serious variations in the computed infiltration rates as compared with a truly nonlinear solution, as will be discussed in Chapter IV.

TABLE 2.1. Nature of Published Numerical Solutions to Vertically Downward Moisture Flow Equation

Source	Date	Upper Boundary Condition	Dependent Variable	Soil Matrix	Basic Purpose of Solution	Numerical Solution Solved	Produced Infiltration Model	Remarks
Klute	1952	ϕ_i = constant	ψ	uniform	θ vs Z	analytical approximation	no	early numerical work
Philip	1956	ϕ_i = constant	Boltzmann transform	uniform	θ vs Z	analytic series approximation	yes	unwieldy
Hanks & Bowers	1962	$\phi_i = \theta_{sat}$	θ	layered	θ vs Z	linearized finite-diff. implicit	yes	
Rubin & Steinhardt	1963	Rainfall = K constant	θ	uniform	θ vs Z	linearized finite-diff. implicit	no	solution good up to ponding only
Liakapolous	1965	Saturated	ψ	uniform	θ vs Z	linearized finite difference	for saturated case only	
Whisler & Klute	1965	Rainfall & Ponding	ψ	uniform	θ vs Z	nonlinear implicit finite-diff.	approximate estimate	
Rubin	1966	Rainfall & Ponding	$V(\psi) = \psi -$ transform	uniform	θ vs Z	quasi-linear implicit finite difference	yes	estimates coefficients with an explicit equation for each time step
Ibrahim	1968	Ponded $\theta = \theta_{sat}$	ψ	uniform	θ vs Z	explicit finite difference	empirical	explicit scheme: accumulated mass balance errors with time
Freeze	1969	Rainfall & ponding	ψ	uniform	θ vs Z	linearized implicit finite difference	rough approximate	

With a few exceptions, these investigators have been concerned with determining moisture profiles at various points in time, rather than obtaining an infiltration model, and the assumptions used reflect this objective. The effect on the accuracy of the solution of such things as size of Δt and Δz increment used, method of linearization or estimation of coefficients, etc., cannot be known if no truly nonlinear solution is available as a comparison. Given a saturated upper boundary condition, there is no way to assess the accuracy of a solution in terms of continuity by summation of change in moisture content. The explicit scheme used by Ibrahim [1967] is an example of this problem. His finite-difference equations were modified to allow a specified rainfall at the surface. Solutions to his equations included a continuity error as shown in Fig. 2.3. The cause is the use of an explicit scheme, which uses values of pressure from the previous time to calculate moisture flow into the z increment ahead, as shown in Fig. 2.4. The solution moves down the column of soil, so that the pressure used for the forward node point at level i is not the same as the pressure used for the same node when the level $i + 1$ is being calculated. This violates continuity.

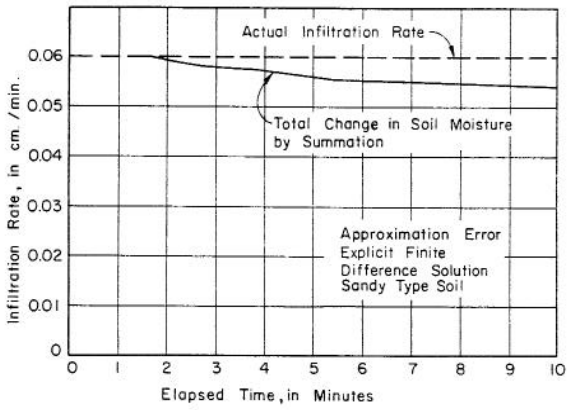

Fig. 2.3. Nature of accumulated error in explicit numerical approximation to equation (2.16).

The linearized implicit schemes do not violate continuity, since a matrix is solved to evaluate pressures at the new time step $t + \Delta t$. The pattern of infiltration and shape of the moisture profile may be affected by the linearization, however, especially near the highly sensitive upper boundary, where small changes greatly affect infiltration rates.

In calculation of infiltration rates from their numerical schemes, most of the investigators cited above encountered difficulty in either point scatter or physical credibility of their curves. Hanks and Bowers [1962] and Whisler [1964], for example, encountered difficulty in scatter of points about an infiltration curve, as in Fig. 2.5. The results of Phuc [1969] are much more widely scattered.

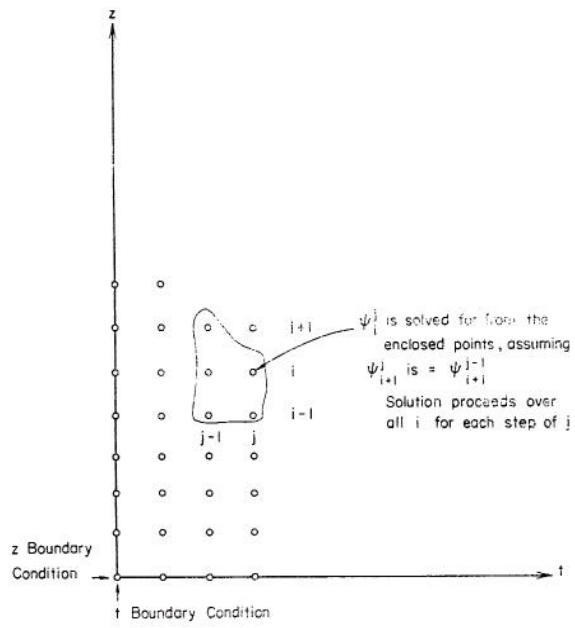

Fig. 2.4. Explicit finite-difference method on the (z,t) grid network.

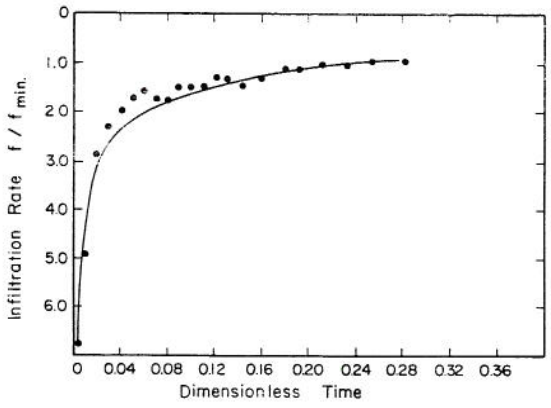

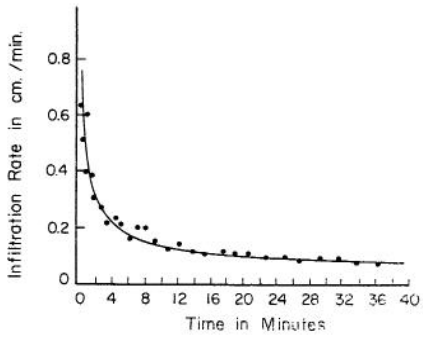

Fig. 2.5. Examples of scatter in the numerical results of Whisler [1964] and Hanks and Bowers [1962].

Field experiments using sprinkling infiltrometers uniformly produce infiltration curves of a general shape, as illustrated in Fig. 2.6. After an initial time in which all applied water is taken into the soil, infiltration rate begins to drop in an exponential- or hyperbolic-type curve, asymptotic to a minimum infiltration rate, which corresponds to the saturated conductivity of the total soil column. When mathematical simulations produce results such as shown in Fig. 2.7, one should conclude that the numerical method of calculating infiltration rates from the soil column is being biased by the numerical scheme. This appears to be the case in the published results of Freeze [1969] and, to some extent, of Whisler and Klute [1965].

None of the investigators discussed herein have reported the effect on the solution of changes in the size of Δz increment used. From experiments discussed in Chapter IV, it appears this is an important factor, especially for the zones where the moisture front is steep. (See Fig. 4.10)

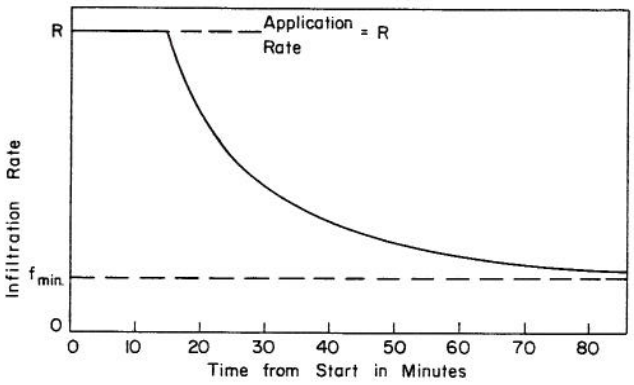

Fig. 2.6. Typical results from sprinkling infiltrometers in field tests.

Many of the methods of solution described in the literature and listed in part in Table 2.1 cannot model a rainfall infiltration boundary condition. Others use a linearized solution method which inadequately models the infiltration rate, or results in severe scatter of the computed values for infiltration rate.

The first objective of this investigation is to develop a finite-difference solution to equation (2.16) which will act as a realistic model of infiltration for physically realizable boundary conditions. It should provide for layered soils, and allow a variation in increment sizes so that a maximum efficiency can be obtained in the solution process. The solution should be obtained in a manner which minimizes the scatter of the computed values of infiltration, and thereby provide a dependable model for use in connection with surface runoff models. The development of the solution method is described in Chapter IV.

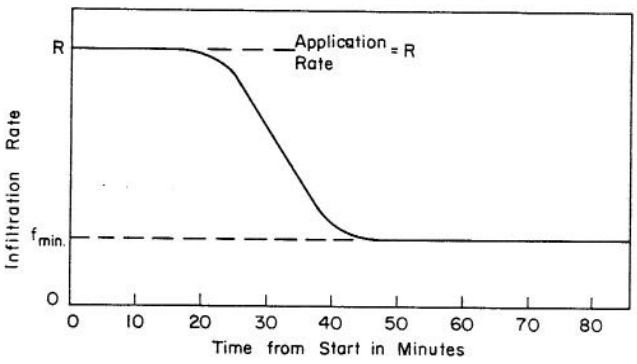

Fig. 2.7. Infiltration rate from the numerical simulation of Freeze [1969].

CHAPTER III

MATHEMATICAL DESCRIPTION OF WATERSHED RESPONSE

Introduction

Water appears on the surface of an infiltrating watershed when the rainfall rate exceeds the infiltration rate. This time varying-difference between rainfall and infiltration may be termed rainfall excess. Water on the soil surface flows under the influence of gravity toward the lower edge of the catchment, and appears as input to a stream or channel. The time variation of this channel input may be termed the catchment hydrograph. This chapter will deal briefly with methods used to mathematically describe the catchment hydrograph from a knowledge of the rainfall excess pattern.

Linear System Approach

The simplest and most common method of watershed response modeling assumes the overland flow process to be a linear system problem, with rainfall excess as input and the watershed hydrograph as the system output. The system behavior is described by the impulse response function or the instantaneous unit hydrograph. Mathematically, this function is the response of the watershed to an instantaneous pulse input. In practice, it must be obtained by using system identification techniques, using measured values of the time series of input (rainfall) and output (runoff) functions.

Nonlinear Fluid Dynamics Description

In fact, the response of a watershed is not linear, and watershed hydraulics can be described more accurately by writing the equations of energy and continuity from fluid mechanics principles. This is a case of nonuniform, unsteady flow, and the governing equations may be stated without derivation as follows:

A. Continuity:

$$\frac{\partial h}{\partial t} + \frac{\partial (uh)}{\partial x} = q(x,t) \qquad (3.1)$$

B. Energy:

$$\frac{\partial u}{\partial t} + u\frac{\partial u}{\partial x} + g\frac{\partial h}{\partial x} = g(S_o - S_f) - \frac{q(x)u}{h} \qquad (3.2)$$

where S_o = slope of the ground surface

S_f = energy gradient

and $u(x,t)$ = local velocity

$h(x,t)$ = local depth

$q(x)$ = local inflow per unit area $[LT^{-1}]$

g = gravitational acceleration .

Either the Manning equation or the Chézy equation may be used to define S_f . In this work, a Chézy form will be used, so that

$$V_o = CH_o^m S_o^{\frac{m+1}{3}} \qquad (3.3)$$

where V_o = velocity at normal depth H_o

S_o = bed slope, and

C = Chézy resistance coefficient or laminar resistance coefficient (C_1) .

This formulation allows a turbulent Chézy relationship when $m = 1/2$, and provides a laminar flow relationship when $m = 2$.

The Kinematic Wave Approximation. The system of equations (3.1), (3.2), and (3.3) can be simplified into the kinematic wave equations for flows where S_o is neither flat nor excessively steep, so that it may be shown that the terms in the left side of equation (3.2) are of the same order of magnitude. Henderson [1963] did this for the case of wide channel flows. By writing equation (3.2) in nondimensional form, Woolhiser and Liggett [1967] showed that the first term on the right side becomes

$$k_* \left(1 - \frac{u_*}{h_*}\right)^{1/m}$$

in which the starred quantities are nondimensional, and

$$k_* = \frac{S_o L_o}{H_o F_o^2}$$

L_o = length of the plane

H_o = normal depth

F_o = Froude No.= $\dfrac{V_o}{\sqrt{gH_o}}$.

From the order of magnitude analysis of Henderson, all terms in the equation have a certain maximum order of magnitude, so that dividing through by k_*, as k_* becomes large, implies $u_*^{1/m} \to h_*$. This means we may use, for large k_*,

$$u = CS_o^{\frac{m+1}{3}} h^m \quad . \tag{3.4}$$

This approximation, combined with equation (3.1), allows solution of the system of equations by a single equation. Define

$$\alpha = CS_o^{\frac{m+1}{3}} \quad , \tag{3.5}$$

so that

$$u = \alpha h^m \quad .$$

Combining this expression with equation (3.1) produces

$$\frac{\partial h}{\partial t} + \alpha(m+1)h^m \frac{\partial h}{\partial x} = q(x,t) \quad , \tag{3.6}$$

which is the kinematic wave equation to be used in this study.

The Kinematic Wave Equation for Cascading Planes. The general watershed considered in this study is made up of a cascade of planes, of different slope, roughness, width, and length, as shown in Fig. 4.1. In this section the kinematic wave equation will be transformed into a nondimensional form applicable to the case of a multiple-plane watershed.

Consider a watershed of n cascading planes, the k^{th} plane having width W_k, length L_k, roughness coefficient C_k, and slope S_k. The normalizing flow will be based on the maximum rainfall excess rate $q_{max}(t)$ as follows:

$$Q_{o(k)} = \frac{q_{max}}{W_k} \sum_{i=1}^{k} W_i L_i \quad .$$

According to equation (3.5)

$$\alpha_k = C_k S_k^{\frac{m+1}{3}} \tag{3.7}$$

Therefore let

$$V_{o(k)} = \alpha_k H_{o(k)}^m \tag{3.8}$$

and

$$Q_{o(k)} = \alpha_k H_{o(k)}^{m+1}$$

or

$$H_{o(k)} = \left(\frac{Q_o}{\alpha}\right)_k^{\frac{1}{m+1}} \quad . \tag{3.9}$$

Then define

$$T_{o(k)} = \frac{1}{V_{o(k)}} \sum_{i=1}^{k} L_i \quad . \tag{3.10}$$

Using (3.9) and (3.10), the variables x, h, and t may be written in nondimensional form as follows:

$$x_{*(k)} = \frac{\sum_{i=1}^{k-1} L_i + x_k}{\sum_{i=1}^{n} L_i} = \frac{\sum_{i=1}^{k-1} L_i + x_k}{L_t} \tag{3.11}$$

where $L_t = \sum_{i=1}^{n} L_i$,

$$h_{*(k)} = \frac{h_k}{H_{o(k)}} = h_k \left(\frac{\alpha}{Q_o}\right)_k^{\frac{1}{m+1}} \quad , \tag{3.12}$$

$$t_{*(k)} = \frac{t}{T_{o(k)}} = \frac{t\, V_o}{\sum_{i=1}^{k} L_i} \quad . \tag{3.13}$$

Now equation (3.6) may be written in nondimensional form:

$$\left(\frac{\partial h_*}{\partial t_*}\right)_k \left(\frac{Q_o}{\alpha}\right)_k^{\frac{1}{m+1}} \frac{1}{T_{o(k)}} + \frac{(m+1)\alpha_k}{L_t} \left(\frac{Q_o}{\alpha}\right)_k^{\frac{m}{m+1}} h_{*(k)}^m \left(\frac{\partial h_*}{\partial x_*}\right)_k \left(\frac{Q_o}{\alpha}\right)_k^{\frac{1}{m+1}} = q_o q_* \quad . \tag{3.14}$$

By dividing to simplify, one can assign

$$q_o = T_{o(k)}^{-1} \left(\frac{Q_o}{\alpha}\right)_k^{\frac{1}{m+1}} = \left(\frac{H_o}{T_o}\right)_k = \frac{q_{max}}{W_k} \frac{\sum_{i=1}^{k} L_i W_i}{\sum_{i=1}^{k} L_i} \quad , \tag{3.15}$$

$$\text{and let } \beta_k = (m+1)\alpha_k \frac{T_o}{L_t} H_o^m = \frac{(m+1)}{L_t} \sum_{i=1}^{k} L_i \quad . \tag{3.16}$$

From these relations, equation (3.14) becomes

$$\left(\frac{\partial h_*}{\partial t_*}\right)_k + \beta_k h_{*(k)}^m \left(\frac{\partial h_*}{\partial x_*}\right)_k = q_*(t) \quad . \tag{3.17}$$

Useful insight into the solution of this equation may be obtained by using a technique known as the method of characteristics (Kibler, 1968). For clarity, the (*) subscripts will be omitted. Taking the total derivative of $h(x,t)$,

$$\frac{dh}{dt} = \frac{\partial h}{\partial t} + \frac{\partial h}{\partial x}\frac{dx}{dt} \quad . \tag{3.18}$$

Equation (3.17) may be rewritten as

$$q(t) = \frac{\partial h}{\partial t} + \beta h^m \frac{\partial h}{\partial x} \quad . \tag{3.19}$$

Comparing like terms from equations (3.18) and (3.19), two ordinary differential equations in h,x,t may be obtained:

$$\frac{dh}{dt} = q(t) \tag{3.20}$$

$$\frac{dx}{dt} = \beta h^m \quad . \tag{3.21}$$

These are known as the characteristic equations for equation (3.17). Equation (3.21) describes the movement of any initial disturbance, including the boundary conditions, in the $x - t$ plane, as shown in Fig. 3.1. Within region A of this figure, flow is uniform unsteady. Outside of the region, flow is nonuniform steady for a step function lateral inflow. Equations (3.20) and (3.21) may be solved to define the characteristic time t_c if $q(t)$ is known. Thus $h(t)$ may be calculated

$$h(t) = \int_o^t q(t)dt, \quad t \le t_c \tag{3.22}$$

and from this

$$x(t) = \int_o^t \beta \left[h(t)\right]^m dt, \quad t \le t_c \quad . \tag{3.23}$$

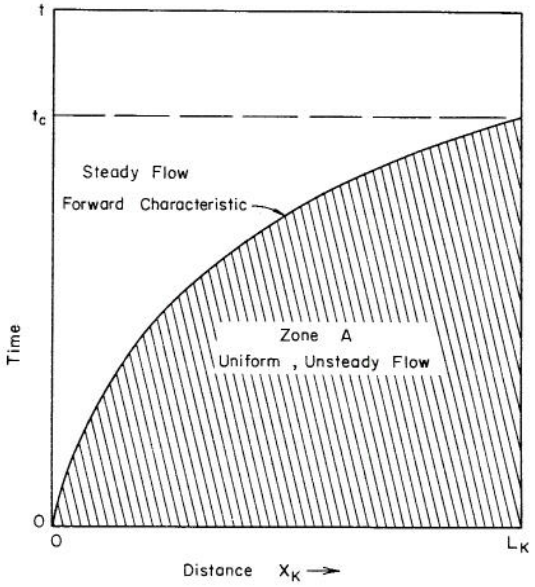

Fig. 3.1. Solution of equation (3.17) in the (x,t) plane.

This expression is analytic when $q(t)$ is an analytic function, but may still be evaluated by numerical integration for any known $q(t)$.

Applications of the Kinematic Wave Equation

Wooding [1965] solved equation (3.17) for certain cases of surface and channel flow where an analytical solution was possible, then extended his work by obtaining numerical solutions for several cases, including the case of a constant value of infiltration rate.

Woolhiser [1967] has obtained a kinematic solution for overland flow on conic sections, a basic geometrical shape in small watersheds. Kibler [1968] treated the problem of the formation of kinematic shocks arising when planes of different slope are cascaded, and the optimization of a single plane to approximate two cascading planes. Foster, Huggins, and Meyer [1968] applied the kinematic wave equations to short field plots with "constant" infiltration rates and demonstrated good comparison with experimental data. Foster [1968] applied the kinematic equations to data from field plots to derive the infiltration rate pattern from knowledge of the plot outflow hydrograph and hydraulic roughness. Burman [1969] utilized the kinematic overland flow equations plus a

Horton infiltration formula to simulate experimental results from several 185' x 200' plots on an experimental farm at Cornell University. He obtained critical parameters for roughness and infiltration by optimization. Then after obtaining the best fit parameters, his simulated hydrographs for selected storms fit the observed data reasonably well.

It is the purpose of this investigation to utilize the kinematic wave equation as a mathematical model of surface hydraulics, with lateral inflow determined by matching the boundary conditions with the equation of soil moisture flow (equation 2.16), such that the difference between rainfall and soil water infiltration becomes lateral input to the surface flow equation. The numerical techniques and theoretical and experimental results will be discussed in the following chapters.

CHAPTER IV

A MATHEMATICAL MODEL OF AN INFILTRATING WATERSHED

Introduction. This chapter describes the development of a mathematical model for the simulation of infiltrating watersheds, from simultaneous solution of the partial differential equations (2.16) and (3.6), subject to compatible boundary conditions. These equations are first written in finite difference form, and then combined for efficient and accurate solution on a digital computer. A discussion of the results of this numerical solution, compared with other finite difference formulations, is given at the end of the chapter.

The solution of each equation proceeds in time and one dimension of distance. For the soil equation, the distance is Z, depth measured from the surface, and the solution is a vector of soil water pressure as a function of (Z,t) and f(t) at the surface. For the surface water flow equation, the distance is x , measured along the surface from the upper edge of each plane, and the solution is a vector of surface water depths as a function of (x,t) . This notation is illustrated in Fig. 4.1.

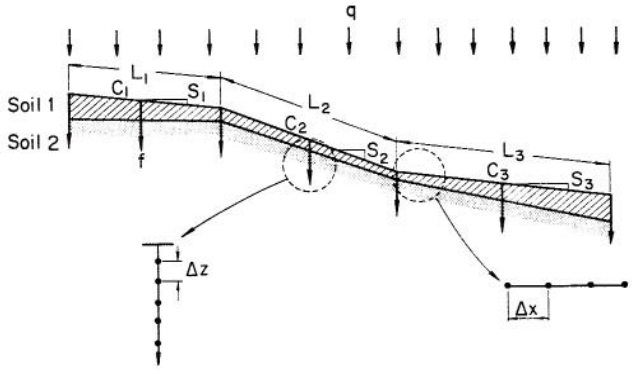

Fig. 4.1. Schematic representation of the mathematical watershed model.

Finite difference notation is illustrated in Fig. 4.2. The Z,t plane (and the x,t plane) is divided into small finite difference segments. Each node is numbered, with i representing points in the Z(or x) dimension and j representing points in the t dimension. Thus ψ_i^j represents the value of $\psi(Z,t)$ at $Z = Z_i$ and $t = t_j$. In the following discussion, superscripts will be used, as above, for time location, and subscripts for distance location.

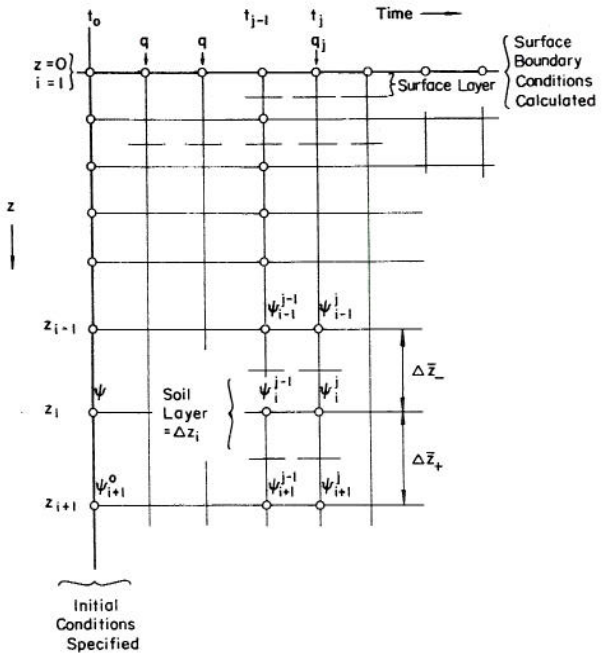

Fig. 4.2. Finite difference solution grid in (z,t) , showing notation used.

Numerical Solution of the Unsaturated Soil Moisture Flow Equation

If equation (2.16) is multiplied by dz , we obtain

$$\frac{\partial}{\partial t}(V_b \phi S_w) = K\frac{\partial}{\partial z}\left(k_r \frac{\partial \psi}{\partial z}\right) dz - K\frac{\partial k_r}{\partial z} dz \qquad (4.1)$$

where V_b is incremental bulk volume, and for this one-dimensional case is simply dz .

Normally the soil pore volume ϕV_b is assumed

constant for solution of this equation. For soils with abundant clay-sized particles, soil swelling may be significant in the change in stored moisture represented by the left-hand side of equation (4.1). A means to account for this swelling may be derived from current theory and experimental observation of the nature of swelling soils.

Swelling Soils. Philip [1969] in a theoretical study of swelling in soils, stated that over a substantial range of moisture contents, as supported by experiment,

$$\frac{\partial e}{\partial \sigma} = \frac{de}{d\sigma} = \alpha \qquad (4.2)$$

where e = voids ratio = $\frac{\phi}{1-\phi}$, α is a constant,

and σ = moisture ratio = $\frac{\theta}{1-\phi}$.

Integrating equation (4.2),

$$e = \sigma\alpha + C_1$$

into which one may substitute definitions of e and σ, and obtain

$$\phi = \alpha\theta + (1 - \phi) C_1 \quad . \qquad (4.3)$$

At $\theta = 0$, $\phi = \phi_{lim}$ so that $C_1 = \frac{\phi_{lim}}{1-\phi_{lim}}$.

ϕ_{lim} is the porosity obtained for oven-dry soil if the relation of (4.3) were true over all ranges of moisture. ϕ_{min} will be taken as the lower limit of ϕ for which (4.3) holds.

Letting $\beta = \alpha(1 - \phi_{lim})$, (4.3) may be written

$$\phi = \beta\theta + \phi_{lim}, \quad \left(\phi > \phi_{min}\right). \qquad (4.4)$$

Soil bulk density ρ_b is a function of porosity ϕ:

$$\rho_b = (1 - \phi)\rho_s \quad ,$$

and define

$$\rho_{b\,max} = (1 - \phi_{lim})\rho_s,$$

where ρ_s is the density of solid grains of soil.

Moisture content w (in volume of water per weight of soil) is a function of θ and bulk density:

$$w = \frac{\theta}{\rho_b} \quad .$$

Using these two relations, equation (4.4) may be transformed into the following form:

$$\frac{1}{\rho_b} = \left[\frac{\beta\rho_s}{\rho_{b\,max}}\right] w + \frac{1}{\rho_{b\,max}} \quad . \qquad (4.5)$$

$\frac{1}{\rho_b}$ is known as the specific porosity, and this equation has the form of the experimental results of Lauritzen [1948] and Lauritzen and Stewart [1941] . It also agrees well with experimental data of Gill [1959], who plotted ρ_b vs. w .

To use equation (4.4) in equation (4.1) as a swelling relationship, θ is replaced by an equivalent statement in terms of saturation:

$$\theta = S_w\phi \quad . \qquad (4.6)$$

Thus equation (4.4) becomes

$$\phi = \frac{\phi_{lim}}{1-\beta S_w} \quad . \qquad (4.7)$$

The left side of equation (4.1) may be expanded as

$$\frac{\partial}{\partial t}(V_b\phi S_w) = \phi S_w \frac{\partial V_b}{\partial t} + V_b \frac{\partial}{\partial t}(\phi S_w) \quad . \qquad (4.8)$$

Because $\frac{\partial V_b}{\partial t}$ should be an order of magnitude smaller than $\frac{\partial(\phi S_w)}{\partial t}$, the derivative may be approximated by

$$\frac{\partial}{\partial t}(V_b\phi S_w) = V_b \frac{\partial}{\partial t}(\phi S_w) \quad . \qquad (4.9)$$

Equation (4.1) will be solved in terms of ψ , so the chain rule of calculus is applied to equation (4.9):

$$V_b \frac{\partial}{\partial t}(\phi S_w) = V_b \frac{\partial}{\partial S_w}(\phi S_w) \frac{S_w}{\partial\psi} \frac{\partial\psi}{\partial t} \quad . \qquad (4.10)$$

Using equation (4.7),

$$\frac{\partial}{\partial S_w}(\phi S_w) = \phi + \frac{\phi(\phi - \phi_{lim})}{\phi_{lim}} = \frac{\phi^2}{\phi_{lim}} \quad . \qquad (4.11)$$

Combining equations (4.11), (4.10), and (4.9) we obtain

$$\frac{\partial}{\partial t}(V_b\phi S_w) = V_b\left(\frac{\phi^2}{\phi_{lim}}\right)\frac{\partial S_w}{\partial\psi}\frac{\partial\psi}{\partial t} \quad , \qquad (4.12)$$

which is valid in the range of S_w for which equation (4.7) holds. Otherwise, ϕ is constant, and

$$\frac{\partial(\phi S_w)}{\partial S_w} = \phi \quad .$$

Finite Difference Formulation. Equation (4.1) may then be written

$$V_b \frac{\partial(\phi S_w)}{\partial S_w} \frac{\partial S_w}{\partial \psi} \frac{\partial \psi}{\partial t} = K \frac{\partial}{\partial z}\left[k_r \frac{\partial \psi}{\partial z}\right] dZ - K \frac{\partial k_r}{\partial z} dz . \qquad (4.13)$$

The initial conditions must be specified in terms of $\psi(x,t)$, and may be any reasonable value as desired:

$$\text{at } t = 0, \qquad \psi_i^o = \psi_{i\,(\text{initial})} .$$

The boundary conditions, for rainfall infiltration, may be specified as follows; for $t > 0$,

$$\text{at } Z = 0, \text{ for } \psi_1^j < 0, \text{ rainfall} = -\left(\frac{\partial \psi}{\partial Z}\right)_1^j K k_{r_1}^j + K k_{r_1}^j$$

$$\text{at } Z = 0, \text{ for } \psi_1^j \geq 0, \ \psi_1^j = h(x,t) = \text{surface depth}$$

$$\text{at } Z = L = \text{water table}, \ \psi_{N_z}^j = 0 .$$

From these equations, a finite difference form based on time and distance averaged quantities can be written, a form known as the Crank-Nicolsen finite difference scheme.

Let $$\frac{V_b}{\Delta t}\left[\frac{\Delta \phi S_w}{\Delta S_w}\right] = \text{STOR}$$

where, from equation (4.11),

$$\frac{\Delta \phi S_w}{\Delta S_w} = \frac{\phi^2}{\phi_{lim}} \quad \text{for } \phi > \phi_{min}; \text{ otherwise} = \phi ,$$

then from equation (4.13),

$$[\text{STOR}]\frac{\Delta S_w}{\Delta \psi} \Delta \psi = \frac{K}{\Delta z}\Delta\left[k_r \frac{\Delta \psi}{\Delta z}\right]\Delta z - K\frac{\Delta k_r}{\Delta z}\Delta z . \qquad (4.14)$$

Let

$$\Delta\psi_+^{j-\frac{1}{2}} = \frac{1}{2}\left[\psi_{i+1}^j - \psi_i^j + \psi_{i+1}^{j-1} - \psi_i^{j-1}\right]$$

and

$$\Delta\psi_-^{j-\frac{1}{2}} = \frac{1}{2}\left[\psi_i^j - \psi_{i-1}^j + \psi_i^{j-1} - \psi_{i-1}^{j-1}\right] \qquad (4.15)$$

where $i = 1,2,3\ldots N_z$ and $j = 1,2,3,\ldots M_t$.

As proposed by Breitenbach, et al, [1968], k_r is selected as the relative permeability at the node from which flow is originating at time t. Thus for Z positive downward, and flow downward we have

$$k_{r_+}^{j-\frac{1}{2}} = \frac{1}{2}\left[k_{r_i}^j + k_{r_i}^{j-1}\right]$$

$$k_{r_-}^{j-\frac{1}{2}} = \frac{1}{2}\left[k_{r_{i-1}}^j + k_{r_{i-1}}^{j-1}\right] ,$$

which are time averages only.

Referring to Fig. 4.2, we define the following quantities:

$$\Delta\bar{z}_+ = z_{(i+1)} - z_{(i)}$$

$$\Delta\bar{z}_- = z_{(i)} - z_{(i-1)} .$$

In accordance with saturated porous media flow theory, saturated conductivity between adjacent layers will be taken as the harmonic mean:

$$K_+ = K_{i+\frac{1}{2}} = \frac{2\Delta\bar{z}_+}{\frac{\Delta z_{(i+1)}}{K_{(i+1)}} + \frac{\Delta z_i}{K_{(i)}}}$$

$$K_- = K_{i-\frac{1}{2}} = \frac{2\Delta\bar{z}_-}{\frac{\Delta z_{(i)}}{\Delta K_i} + \frac{\Delta z_{(i-1)}}{\Delta K_{(i-1)}}} .$$

Utilizing these definitions, (4.14) may be expanded, reversing sides:

$$\left[K_+ \frac{k_{r_+}\Delta\psi_+}{\Delta\bar{z}_+} - K_+ k_{r_+} - \frac{K_- k_{r_-}\Delta\psi}{\Delta\bar{z}_-} + K_- k_{r_-}\right]_i^{j-\frac{1}{2}} + Qp_i = [\text{STOR}]_i^{j-\frac{1}{2}}\left[\frac{\Delta S_w}{\Delta\psi}\right]_i^{j-\frac{1}{2}}\left[\psi_i^j - \psi_i^{j-1}\right] . \qquad (4.16)$$

Where Qp_i is input to that node from outside, used only at the surface to provide rainfall input up to ponding: $Qp_i = 0$ for $i > 1$.

Substituting expressions (4.15) into (4.16),

$$K_{i+\frac{1}{2}} k_{r_+}^{j-\frac{1}{2}}\left[\frac{\psi_{i+1}^j - \psi_i^j + \psi_{i+1}^{j-1} - \psi_i^{j-1}}{2\Delta\bar{z}_+}\right] - K_{i-\frac{1}{2}} k_{r_-}^{j-\frac{1}{2}}\left[\frac{\psi_i^j - \psi_{i-1}^j + \psi_i^{j-1} - \psi_{i-1}^{j-1}}{2\Delta\bar{z}_-}\right]$$
$$- K_{i+\frac{1}{2}} k_{r_+} + K_{i-\frac{1}{2}} k_{r_-} = [\text{STOR}]_i^{j-\frac{1}{2}}[\text{SL}]_i^{j-\frac{1}{2}}\left[\psi_i^j - \psi_i^{j-1}\right] - Qp_i . \qquad (4.17)$$

Where SL is defined at i, j as $\left[\frac{\Delta S_w}{\Delta\psi}\right]_i^j$.

Equation (4.17) is now rearranged so that only terms of ψ^j are on the left side:

$$\frac{K_{i+\frac{1}{2}}k_{r_+}}{2\Delta\bar{z}_+}\left[\psi_{i+1}^{j}-\psi_i^{j}\right]-\frac{K_{i-\frac{1}{2}}k_{r_-}}{2\Delta\bar{z}_-}\left[\psi_i^{j}-\psi_{i-1}^{j}\right]-[STOR]_i^{j-\frac{1}{2}}[SL]_i^{j-\frac{1}{2}}\psi_i^{j}$$

$$=-[STOR]_i^{j-\frac{1}{2}}[SL]_i^{j-\frac{1}{2}}\psi_i^{j-1}-Qp_i-\frac{K_{i+\frac{1}{2}}k_{r_+}}{2\Delta\bar{z}_+}\left[\psi_{i+1}^{j-1}-\psi_i^{j-1}-2\bar{z}_+\right]$$

$$+\frac{K_{i-\frac{1}{2}}k_{r_-}}{2\Delta\bar{z}_-}\left[\psi_i^{j-1}-\psi_{i-1}^{j-1}-2\Delta\bar{z}_-\right] \quad . \qquad (4.18)$$

Let $RHS_i^{j-\frac{1}{2}}$ represent the right-hand side of equation (4.18), and separate the ψ terms of the left side:

$$\left\{\frac{K_{i-\frac{1}{2}}k_{r_-}}{2\Delta\bar{z}_-}\right\}\psi_{i-1}^{j}-\left\{\frac{K_{i+\frac{1}{2}}k_{r_+}}{2\Delta\bar{z}_+}+\frac{K_{i-\frac{1}{2}}k_{r_-}}{2\Delta\bar{z}_-}+[STOR]_i^{j-\frac{1}{2}}[SL]_i^{j-\frac{1}{2}}\right\}\psi_i^{j}$$

$$+\left\{\frac{K_{i+\frac{1}{2}}k_{r_+}}{2\Delta\bar{z}_+}\right\}\psi_{i+1}^{j}=RHS_i^{j-\frac{1}{2}} \quad . \qquad (4.19)$$

This represents a set of N linear equations in N variables, of the form

$$a_i\psi_{i-1}+b_i\psi_i+c_i\psi_{i+1}=RHS_i \quad ; \; 1\le i\le N \quad , \qquad (4.20)$$

or as a matrix equation

$$[A]\vec{\psi}=\vec{RHS} \quad . \qquad (4.21)$$

It remains to apply the appropriate boundary conditions to form equations of the form (4.20), so that the $N \times N$ matrix [A] and the N-dimensional vector RHS may be completed.

Upper Boundary Conditions. For the upper boundary, equation (4.20) becomes

$$b_1\psi_1+c_1\psi_2=RHS_1 \quad .$$

The rainfall upper boundary condition refers to node 1, which is at the surface. We may write an expression for flow at this point, including the change in storage in the upper layer (see Fig. 4.2), analagous to equation (4.18);

$$\frac{K_{1\frac{1}{2}}k_{r_+}}{2\Delta\bar{z}_+}\left[\psi_2^{j}-\psi_1^{j}\right]-[STOR]_1^{j-\frac{1}{2}}[SL]_1^{j-\frac{1}{2}}\psi_1^{j}=$$

$$-[STOR]_1^{j-\frac{1}{2}}[SL]_1^{j-\frac{1}{2}}\psi_1^{j-1}-Qp_1-\frac{K_{1\frac{1}{2}}k_{r_+}}{2\Delta\bar{z}_+}\left[\psi_2^{j-1}-\psi_1^{j-1}-2\Delta\bar{z}_+\right] . \qquad (4.22)$$

The ponded upper boundary condition simply specifies that $\psi_1^j = h(x)$ which is the depth of water at the surface. In this case the first equation in the set (4.20) is for layer $i = 2$, and terms in ψ_1^j are placed on the right side of the equation as known values.

For the case where saturation has proceeded below the surface, the relationship for ψ vs. S_w is constant, that is, $S_w(\psi \ge 0)$ = constant, and likewise, $k_r(\psi \ge 0)$ = constant. When these relationships are used in equation (4.13), it reduces to an expression of Darcy's law. Below some point n near the surface, the soil will be unsaturated, and as long as the curves of ψ vs. S_w vs. k_r are extended to include positive pressures of ψ, the transition from unsaturated to saturated may be described by equation (4.13) and, in finite difference form, equation (4.19). The upper boundary condition will be $\psi_1^j = h(x)$, and $\frac{\partial S_w}{\partial t}$, for $i < n$ will be 0. From Fig. 4.3, by Darcy's law,

$$\psi_n^j = z(n)\left[1-\frac{f(t)}{K_n}\right]+h(x) \quad . \qquad (4.23)$$

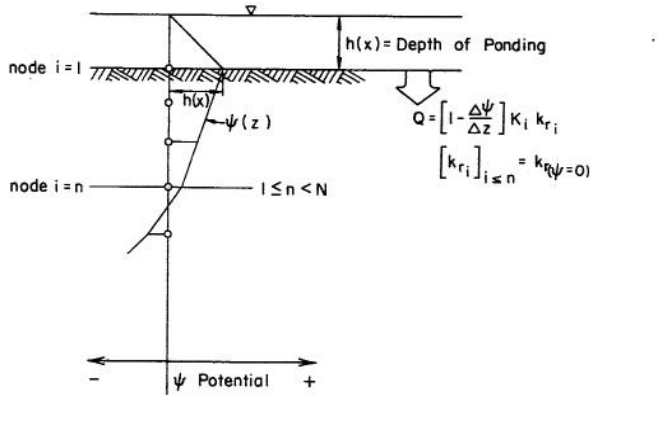

Fig. 4.3. Pressure relations when water is ponded on the soil surface.

The finite difference upper boundary condition may then be written as equation (4.19), with all $\psi_{i-1}^j = \psi_n^j$ terms moved to the right side, and $\psi_n^j = \psi_n^{j-1}$ determined by equation (4.23). The first equation in the set (4.20) is for $i = n+1$.

Lower Boundary Conditions. For all cases where the influence of the upper boundary perturbation has reached only part way down the soil column, a truncated matrix is solved. A point m is chosen such that for $i \ge m$, $\left|\psi_i^{j-1} - \psi_i^0\right| \le \epsilon$, where ϵ is a very

small error value. Thus an equation of the form (4.18) is written for $i = m$, and all terms in $m+1$ are known and set on the right side of the equation. When moisture reaches the water table, the same lower boundary equation applies, except that $\psi^j_{m+1} = 0$.

Inversion of the Matrix [A]. Matrix [A] in equation (4.21) is a diagonally dominant tri-diagonal matrix as shown below:

$$\begin{bmatrix} b_1 & c_1 & & & & \bigcirc \\ a_2 & b_2 & c_2 & & & \\ & a_3 & b_3 & c_3 & & \\ & & & & & \\ & & & a_{m-1} & b_{m-1} & c_{m-1} \\ \bigcirc & & & & a_m & b_m \end{bmatrix} \begin{bmatrix} \psi_1 \\ \psi_2 \\ - \\ - \\ - \\ - \\ \psi_m \end{bmatrix} = \begin{bmatrix} rhs_1 \\ rhs_2 \\ - \\ - \\ - \\ - \\ rhs_m \end{bmatrix} . \qquad (4.24)$$

This is a case which allows solution for the column vector ψ by a simple recursion algorithm for Gauss elimination as given by Varga [53]:

$$w_1 = \frac{c_1}{b_1}; \quad w_i = \frac{c_i}{b_i - a_i w_{i-1}}, \qquad 2 \le i \le m-1$$

$$g_1 = \frac{rhs_1}{b_1}; \quad g_i = \frac{rhs_i - a_i g_{i-1}}{b_i - a_i w_{i-1}}, \qquad 2 \le i \le m$$

$$\psi_m = g_m; \quad \psi_i = g_i - w_i \psi_{i+1}, \qquad 1 \le i \le m-1 . \qquad (4.25)$$

Solution of Equation (4.14) for a Given Time Step. The following items summarize the main features of the solution process.

1. Soil Data Input.

For calculation of values of k_r, $\Delta S/\Delta\psi$, and all other coefficients in equation (4.18), the hydraulic properties of the soil must be known. Curves of ψ vs. S_w vs. k_r are used in the form of empirical curves defined by specific data points. As many points as desired may be used to define the curve, and the data are used in the form of a three-column table. Intermediate points are found by linear interpolation, and any one of the three variables may be used to find a corresponding value for either of the other two. A computer subroutine is used for this calculation; a separate subroutine allows calculation of the slope of the ψ vs. S_w curve at any point, using parabolic interpolation. Where $\Delta\psi$ over a time step becomes greater than a given lower limit, $\Delta\psi/\Delta S$ is found by using chord approximation, as shown in Fig. 4.4.

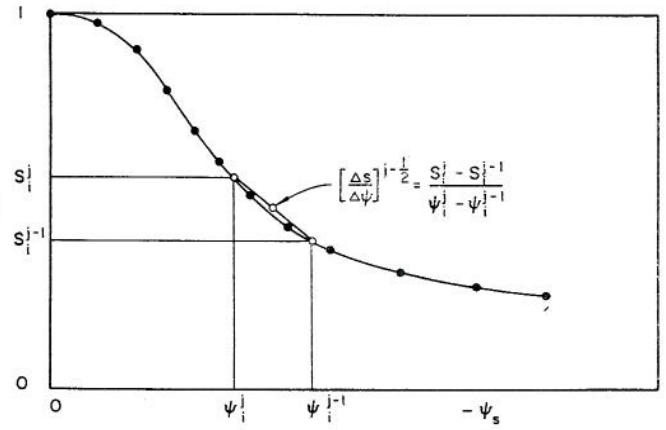

Fig. 4.4. Slope determined by the chord method from moisture tension data.

2. Iteration

It is important to note that the quantities $(STOR)_i^j$, $(SL)_i^j$, and $k_{r_i}^j$ are dependent on the value of ψ_i^j -- that is, the equation (4.14) is highly nonlinear. The quantities listed above must each be evaluated by the hydraulic properties of the soil, namely, relations among k_r, S_w, and ψ, as discussed in Chapter II.

To properly treat this nonlinearity an iterative procedure must be used as follows:

a. An initial estimate of ψ_i^j, $i = 1, m$ is made, and values of $k_{r_i}^j$ $(STOR)_i^j$, and $(SL)_i^j$ are found from soil hydraulic relations.

b. The coefficients a, b, and c are computed and matrix equation (4.24) is solved.

c. The values of ψ_i^j from step (b) are compared with the estimated values used in step (a) for coefficients a_i, b_i, and c_i, and if each agrees within a given error criterion, equation (4.24) is considered solved.

d. If the estimated ψ_i^j are sufficiently different from the solved ψ_i^j from step (b), the new values of ψ_i^j are used to calculate new a_i, b_i, and c_i, and step (b) is repeated.

There is no known mathematical proof that the iteration procedure given above is generally convergent. Formal proof of the convergence of iteration of such systems of nonlinear equations is beyond the scope of this work (see Smith, 1970). Considerable study was made to determine the empirical nature of this convergence, with the purpose of minimizing the number of iterations necessary to achieve agreement between assumed and calculated values of ψ_i^j. The nature of the convergence or divergence of such a scheme appears to be dependent on the type of difference equation used (see end of this chapter), the finite grid dimensions, and the local shape of the $S - \psi - k_r$ properties of the soil. For the Crank-Nicolsen difference scheme, iteration seems to

generally converge in a manner shown in Fig. 4.5. From these results, two modifications were made in the iteration procedure outlined above. First, after three iterations, the estimated ψ_i^j was "damped" by a weighted average with the last ψ_i^j. Secondly, convergence was tested by comparison with both the results of the last iteration and the results of the next-to-last iteration, to detect small order cycling convergence, which was common. In case $\Delta_2\psi_i^j$, shown in Fig. 4.5, becomes sufficiently small, ψ_i^j (estimate) is taken as the mean of the ψ_i^j from the last two interations.

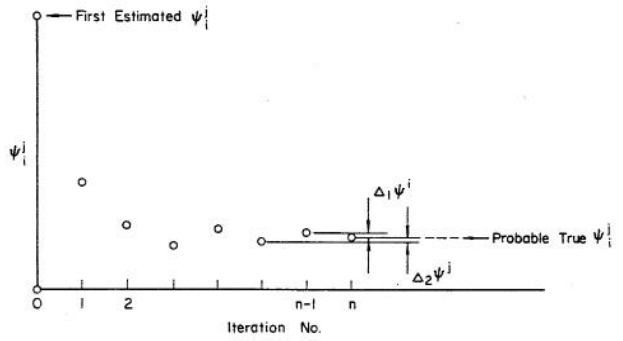

Fig. 4.5. General manner of convergence for the iterated Crank-Nicolsen difference solution to equation (4.13).

3. Selection of Size of Depth and Time Increments.

The difference equation (4.13) becomes the differential equation as $\Delta z \to dz$ and $\Delta t \to dt$. Thus the quality of the difference solution is a function of the fineness of the grid used in the solution. Selection of both Δt and Δz is a process of optimizing, since smaller increments will considerably increase computation time, and too large increments will cause inaccuracies in the results or divergence in iteration. Given a reasonably small Δz, Δt can be chosen arbitrarily small, but beyond a certain lower limit, the solution cannot be improved without changing Δz as well.

Depth Increments. Computations using different Δz sizes demonstrated clearly the importance of making the Δz network as small as practical. The results are presented and discussed at the end of this chapter. For purposes of an infiltration model, the Δz mesh is made smaller toward the surface both to define accurately the time of ponding and inception of runoff, and to define properly the steeply varying pressures which are encountered in this zone as the moisture begins to disperse into the soil column.

Time Increment. If k_r and $\partial S/\partial\psi$ were constant in equation (4.13), it would be a linear partial differential equation, and there would be no restrictions on the time step in the Crank-Nicolsen difference scheme. In nonlinear difference schemes, such as used here, such coefficients are assumed to have linearly averaged values over the time step chosen. Neither of these values actually varies in a linear fashion over a Δt increment, so that the Δt used will affect the solution accuracy. Experimentation with the numerical solution demonstrated that the nonlinear changes of k_r affect the computed accuracy of the resulting distribution of moisture over the soil column, while nonlinear changes of $\Delta S/\Delta\psi$ are most noticeable in the accuracy of integrated moisture change over the time step, e.g., continuity errors.

On this basis, the limiting criterion used for time step selection was the change in $\Delta S/\Delta\psi$ over the time step. This was estimated from the change during the previous time step and the local change in curvature $(\Delta^2 S/\Delta\psi^2)_i^j$ of the soil moisture tension relation. Use of such a criterion allows longer time steps when rainfall is low and saturation changes are slow, or when the moisture-tension curve changes slope more gradually. This minimizing of the local curvature of the $S_w - \psi$ relationship also insures the goodness of the approximations upon which the Crank-Nicolsen averaging scheme is based.

4. Calculation of Infiltration

Infiltration rates may be calculated by equation (4.23) when n becomes 1, that is, when the surface becomes saturated. The value obtained should correspond within a reasonable criterion of accuracy to the moisture change in the soil column over the current time step, calculated by

$$f(t) = \frac{1}{\Delta t} \sum_{i=1}^{N} z_i \phi_i^j \left[S_w^j - S_w^{j-1} \right]_i \qquad (4.26)$$

The Crank-Nicolsen finite difference scheme was chosen as a result of extensive comparisons of the infiltration rate calculated by the above two methods for the schemes tested. This comparison, for $t <$ time of ponding, serves as a continuity test on the performance of the numerical scheme.

Numerical Solution of the Surface Water Flow Equation

Finite Difference Equation. Equation (3.17) is solved by an explicit finite difference method known as the single-step Lax-Wendroff scheme. Using the notation presented at the beginning of this chapter, and illustrated in Figs. 4.1 and 4.2, equation (3.17) is written as a second-order explicit finite difference scheme. First $h(x,t)$ is expanded in a Taylor series:

$$h(x, t + \Delta t) = h(x, t) + \Delta t \frac{\partial h}{\partial t} + \frac{\Delta t^2}{2} \frac{\partial^2 h}{\partial t^2} + 0\left[\Delta t^3\right]. \qquad (4.27)$$

From equation (3.17)

$$\frac{\partial h}{\partial t} = -\beta h^m \frac{\partial h}{\partial x} + q = \frac{\partial}{\partial x}\left[\frac{-\beta h^{m+1}}{m+1}\right] + q \quad ,$$

and from this

$$\frac{\partial^2 h}{\partial t^2} = \frac{\partial}{\partial t}\left[\frac{\partial}{\partial x}\left(\frac{-\beta h^m}{m+1}\right) + q\right]$$

$$= \frac{\partial}{\partial x}\left[\frac{\partial}{\partial t}\left(\frac{-\beta}{m+1} h^{m+1}\right)\right] + \frac{\partial q}{\partial t}$$

$$= \frac{\partial}{\partial x}\left\{-\beta h^m\left[\frac{\partial}{\partial x}\left(\frac{-\beta}{m+1} h^{m+1} + q\right)\right]\right\} + \frac{\partial q}{\partial t} .$$

Thus, from (4.27),

$$h(x, t+\Delta t) = h(x,t) - \Delta t\left[\frac{\partial}{\partial x}\left(\frac{\beta h^{m+1}}{m+1}\right) - q\right]$$

$$+ \frac{\Delta t^2}{2}\left\{\frac{\partial}{\partial x}\left[\beta h^m \frac{\partial}{\partial x}\left(\frac{\beta}{m+1} h^{m+1} - q\right)\right] + \frac{\partial q}{\partial t}\right\} . \qquad (4.28)$$

Now an explicit finite difference form of equation (4.28) is written:

$$h_i^j = h_i^{j-1} - \Delta t\left\{\frac{\beta}{m+1}\left[\frac{(h_{i+1}^{j-1})^{m+1} - (h_{i-1}^{j-1})^{m+1}}{2\Delta x}\right] - \frac{1}{2}\left(q_{i+1}^{j-1} + q_{i-1}^{j-1}\right)\right\}$$

$$+ \frac{\Delta t^2}{2}\left\{\frac{\beta}{2}\frac{\left[(h_i^{j-1})^m + (h_{i+1}^{j-1})^m\right]}{\Delta x}\left[\frac{\frac{\beta}{m+1}(h_{i+1}^{j-1})^{m+1} - \frac{\beta}{m+1}(h_i^{j-1})^{m+1}}{\Delta x}\right.\right.$$

$$\left. - \frac{1}{2}\left(q_{i+1}^{j-1} + q_i^{j-1}\right)\right] - \frac{\beta}{2}\frac{\left[(h_{i-1}^{j-1})^m + (h_i^{j-1})^m\right]}{\Delta x}$$

$$\left[\frac{\frac{\beta}{m+1}(h_i^{j-1})^{m+1} - \frac{\beta}{m+1}(h_{i-1}^{j-1})^{m+1}}{\Delta x} - \frac{1}{2}\left(q_i^{j-1} + q_{i-1}^{j-1}\right)\right]$$

$$\left. + \frac{(q_i^j - q_i^{j-1})}{\Delta t}\right\} . \qquad (4.29)$$

This formulation has been shown by Kibler and Woolhiser [1970] to be stable for

$$\frac{\Delta t}{\Delta x} < \frac{1}{\beta h^m} \qquad (4.30)$$

Boundary Conditions. For the upper boundary, the conditions are, for the k^{th} plane,

$$k = 1, \quad h_{(i=1)} = 0 \text{ for all } t$$

$$k > 1, \quad h_{(i=1)k} = h_{(i=N)k-1}, \text{ for } w_k = w_{k-1} .$$

If $w_k \neq w_{k-1}$, $h_{(i=1)k}$ is specified to preserve continuity of flow, based on $q_{(k-1)}$. The solution proceeds by planes from the upper end, and results from the $(k-1)^{st}$ plane are stored as upper boundary conditions for the k^{th} plane. For the lower boundary, a first-order difference approximation is used, whereby

$$h_{i=N}^j = h_{i=N}^{j-1} - \frac{\Delta t}{m+1}\left\{\frac{\beta}{2}\frac{\left[(h_N^{j-1})^{m+1} - (h_{N-1}^{j-1})^{m+1}\right]}{\Delta x} - \frac{q_N^{j-1} + q_{N-1}^{j-1}}{2}\right\} \qquad (4.31)$$

At the start, of course, the watershed is dry, and the initial conditions are $h_i^{j=1} = 0$ for $1 < i < N_x$.

Combination of the Numerical Models of Soil Moisture Flow and Surface Water Movement

General Structure of the Numerical Solution. The watershed modeled has been described schematically in Fig. 4.1. The finite difference approximation to this scheme is illustrated in Fig. 4.6. Soil conditions as well as initial moisture conditions may vary along the plane, so that although soil moisture movement is described only in the vertical direction, horizontal variations are modeled by a discrete distribution of points along the plane. These points are equally spaced, and in Fig. 4.6 are represented by M_k points, where M_k may vary from 1 to any number, dependent on the scale of horizontal variations, as well as available computer memory and efficiency of computer time desired.

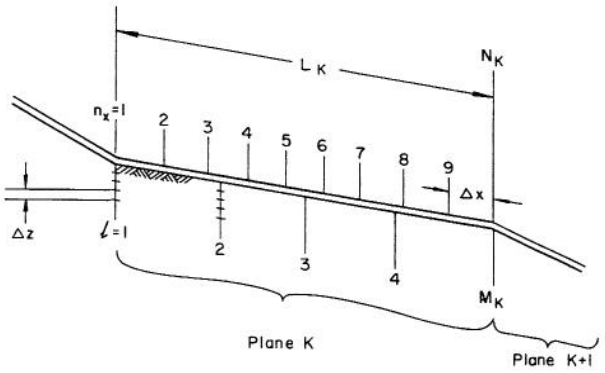

Fig. 4.6. Finite difference grid approximation for the infiltrating watershed.

Each of the M_k points provides a value of $q(x,t)$ for input to the overland flow model. The overland flow model for plan k will require N_k divisions for the finite difference approximation, where $N_k \cdot \Delta x = L_{(k)}$. For efficiency, it is desirable that N_k not be restricted to equal M_k . Thus the two numerical solutions are matched by interpolation at the surface. If $M_k = 1$, for example, $q(1) = q(2) = \ldots q(N_k) = q$. For $M_k = 2$, the soil model is solved at the ends of each plane,

and $q(n)$ is found by linear interpolation. A subroutine is used for this interpolation and provides for any value of N_k and M_k such that $M_k \geq 1$, and $N_k \geq 3$.

The matrix equation (4.21) is solved at each time step for each point on the plane, after which the explicit equation (4.29) for surface flow is solved, using the same time step. Each time step is chosen considering both condition (4.30) and the criteria for the moisture flow time step discussed above.

Operational Logic: 1. Saturation. For a rainfall (RF), either constant or varied such that $RF > K_s$, some time t_s will be reached at which the surface becomes saturated, that is $\psi_1^j = 0$. After this point, runoff will begin, and infiltration is calculated by equation (4.23) and by equation (4.26). Water will begin to "pond" $(h(x) > 0)$, and ψ_1^j will be calculated by equation (4.29). Rainfall excesses are distributed along the plane as described above. When a depth of water exists on the surface, it is also considered as available moisture, in addition to rainfall; thus if the lower watershed soil does not saturate as soon as the upper area, for example, the surface water equations will predict a flow of water onto the lower area, and potential inflow rate to the soil model will be $RF + h(x)/\Delta t$. This is only a crude method for dealing with the advancing front problem, well-known in irrigation studies.

2. Recession. When, after runoff has begun, the rainfall rate drops below infiltration rate, $h(x,t)$ will be decreased both by drainage predicted from the surface flow equation and by infiltration of the surface storage into the soil. Infiltration decreases surface storage at the potential rate, (when after rainfall is less than $K_s(\Delta\psi/\Delta z)_i$) until the depth at that point on the surface reaches 0. In this case, $q(x,t)$ in the surface flow equation will be negative until $h(x,t)$ becomes ≤ 0. Conversely, the soil equation is solved for the saturated upper boundary condition until $h(x,t)$ reaches 0, after which the soil surface desaturates. A $Qp_1 = RF$ upper boundary condition (drainage) is then used, as long as RF remains less than potential f, and $\psi_1 \leq 0$.

A logical network, shown in a general schematic in Fig. 4.7, is used to detect the current condition of the surface for proper assignment of boundary conditions at the start of a new time step. When ψ_1^{j-1} is sufficiently near 0, it is necessary to know whether the soil is saturating or desaturating. It is also necessary to know when the time step should be changed prior to ponding to insure that the point in time when $\psi_i^j = 0$ is not overshot by the time step, and a smooth transition of boundary conditions can occur. If the watershed is undergoing recession, conditions must be investigated to see if the available surface water is less than the potential infiltration at that time, so that the upper boundary condition may be reset to unsaturated for the new time step.

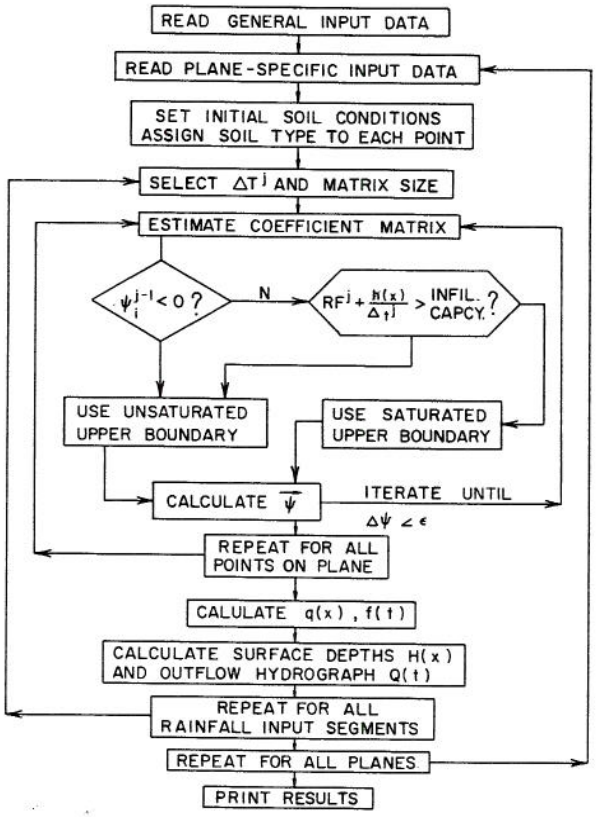

Fig. 4.7. General logical network for computer solution of equations (4.18) and (4.30).

Experiments on Numerical Methods and Solution Sensitivity.

The numerical procedure presented previously is the most satisfactory of several finite-difference formulations of equation (2.16) that were tested. The investigation of methods of numerical solution of equation (2.16) constituted the first part of this study.

Finite-difference Formulations. The first method used was an explicit scheme similar to that used by Ibrahim [1967], but allowed for rainfall as the upper boundary condition. The rainfall boundary condition was described by a difference equation with pressures at the upper two nodes as unknowns. This was solved simultaneously with a difference equation for nodes 1, 2, and 3, similar to equation (4.18), in which $\psi_3^j = \psi_3^{j-1}$. Solution for the remaining nodes proceeded sequentially with ψ_{i+1}^j assumed $= \psi_{i+1}^{j-1}$ when solving for ψ_i^j. As shown in Fig. 2.2, the solution diverges with time because of the assumption stated above. Such divergence can be minimized by taking Δt sufficiently small, but availability of

the rapid matrix solution algorithm (4.25) allows equal or better speed by means of an implicit formulation.

Several implicit methods were tested empirically to determine which appears to be the best method. One way to write a finite-difference form of equation (4.1) is to use coefficients evaluated at the end of the time step. This method is referred to as a fully implicit formulation. In this case, the coefficients $[SL]_i$, $[STOR]_i$ would be evaluated using ψ_i^j rather than $\frac{1}{2}(\psi_i^j + \psi_i^{j-1})$. An example of the results of such a scheme in terms of integrated infiltration rates is shown in Fig. 4.8. The use of coefficients evaluated at the new time step causes the bias in the infiltration, which would not be detected if only moisture profiles were computed. Similarly, the linearized formulations, used by several previous investigators (Chapter II), where coefficients are calculated at the beginning of the time step (from the previous values of ψ) causes an opposite bias in the infiltration rate.

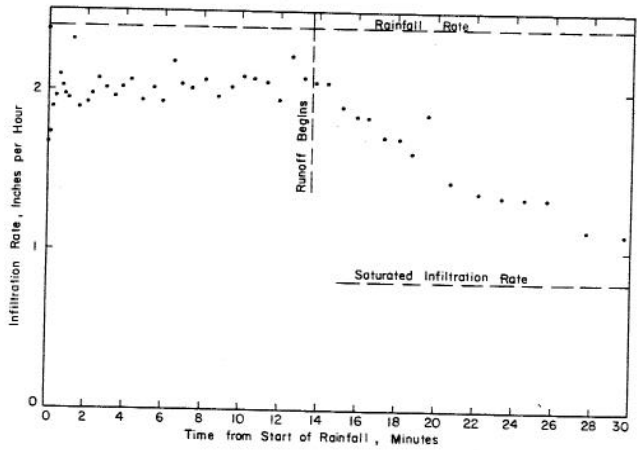

Fig. 4.8. Example of computed infiltration rates using a fully implicit difference formulation.

Because the saturation-depth curve becomes very steep for infiltration into dry soils, it is reasonable that a second-order finite-difference formulation might better approximate the partial differential equation (4.1). Such a method was derived in a manner similar to the second-order Lax-Wendroff difference method in Chapter III, starting with a Taylor series expansion. Iterative solution of this implicit formulation proved somewhat difficult, as the iteration was generally not naturally convergent. Furthermore, the scheme proved unstable, as illustrated by the sample results of Fig. 4.9. Unfortunately, the stability and convergence properties of the nonlinear finite-difference formulas are difficult if not impossible to determine analytically, and such trial and error methods are unavoidable.

Sensitivity of the Numerical Solution. Given a watershed model system, with rainfall rate as the input and infiltration rates and runoff rates as output, it is of interest to determine the sensitivity of the

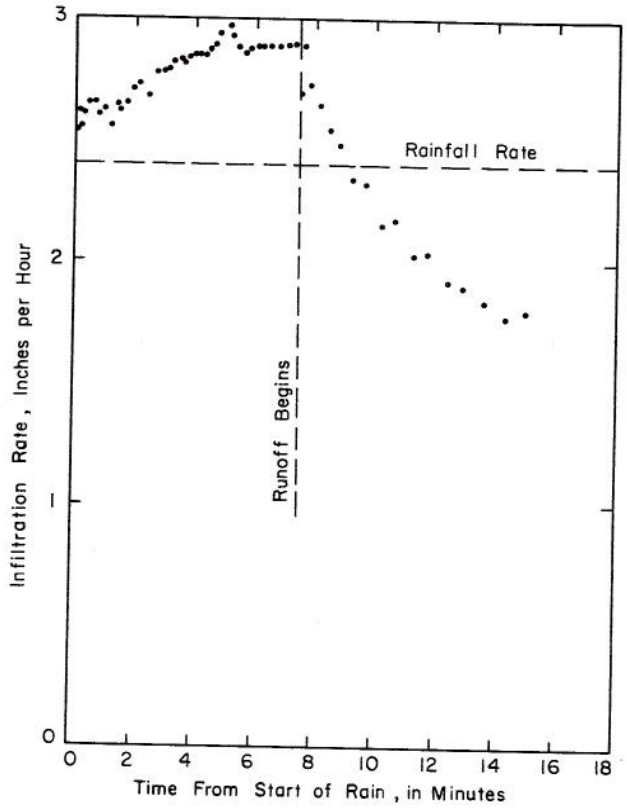

Fig. 4.9. Example of computed infiltration rates using a second order difference formulation.

system to small variations in the system parameters. The important system parameters in this model are the size of the time step, the size of the depth and length increments, the saturated conductivity of the soil, and the hydraulic properties of the unsaturated soil, i.e., the $k_r - S_r - \psi$ relations.

The role of the size of the time step has been discussed previously in this chapter. In some cases, the iterative process will converge for quite large time steps, but they must be limited to accurately reflect the nature and degree of nonlinearity and the scale of time and space variations modeled.

The effect of the size of the depth increment on the numerical solution of equation (2.16) has received scant attention in literature. From the results of this study, it appears to play a critical role. Fig. 4.10 shows the effect on the soil moisture profile of three different sizes of ΔZ in the solution of equation (4.17). The moisture front becomes progressively steeper as the Z increment size is reduced. The corresponding effect on infiltration rates is shown in Fig. 4.11. The time of inception of runoff is markedly affected by the choice of ΔZ size, and the difference in infiltration rates is even more marked than the saturation profiles.

The general effect of changes in K_s , the saturated conductivity, on the infiltration rate is

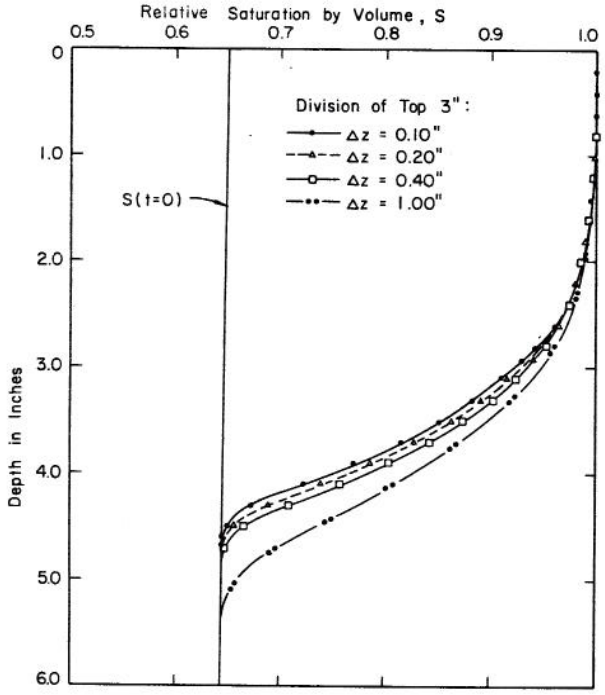

Fig. 4.10. Example of the effect of ΔZ size on computed moisture saturation profile.

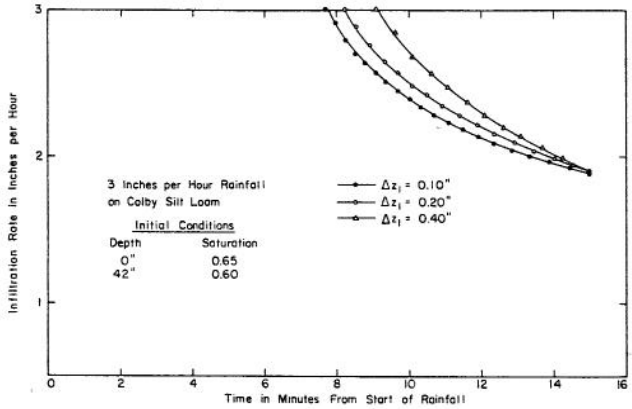

Fig. 4.11. Example of the effect of ΔZ size on computed infiltration rate.

illustrated in Fig. 4.12. For an increase in K_s, the infiltration curve is shifted in a negative direction in both the f dimension and the t dimension. This appears to be an important property in terms of the sensitivity of the overall infiltration curves. A lower K_s results in a steeper saturation-depth curve, at least at the early stages of infiltration, as a noticeable front is moving down the soil profile. This is associated with the earlier inception of runoff.

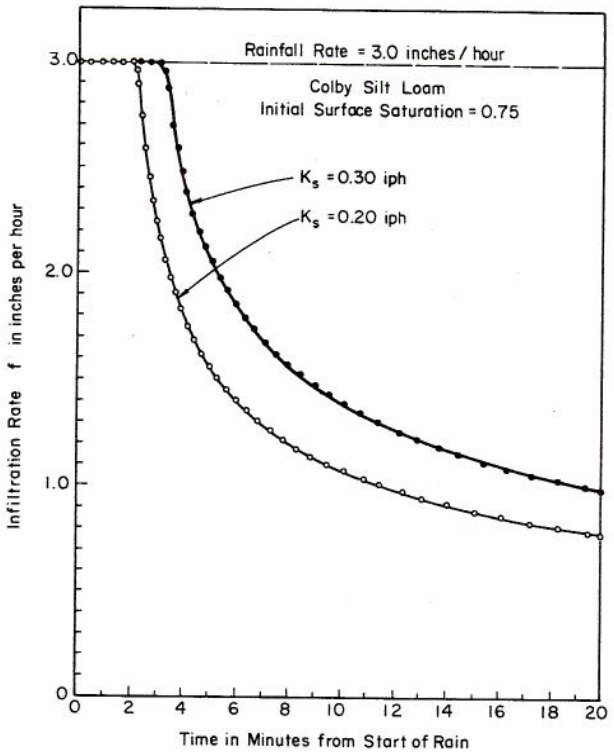

Fig. 4.12. Example of the effect of K_s on infiltration rate.

It is beyond the scope of this study to investigate in detail the sensitivity of the numerical solution to various changes in the hydraulic relations of unsaturated porous media. Some observations on sensitivity gathered in the experimentation of this work will be presented here briefly. In general, the numerical results in this work concur with those published by Hanks and Bowers [1963]. Unquestionably, considerable work is needed to investigate solution sensitivity.

In describing the effect of changes in the assumed $S - k_r - \psi$ relations, one should keep in mind the interdependence of those relations. That is, in an actual soil, if the $S - \psi$ curve is somehow changed, the physical means used to effect the change will also necessarily change the $k_r - \psi$ relationship. Therefore, the effect of a shift in the $S - \psi$ curve shown in Figs. 4.13, 4.14 and 4.15 comes from changes in both the $S - \psi$ and $k_r - \psi$ relations. For Curve A less moisture is stored in the profile in the time t_i from start of rain to when surface saturation ($\psi_1 = 0$) occurs, and thus t_i is less than for curve B. In addition, the permeability curve for saturation curve A will be shifted to the left with respect to curve B, and the result is a steeper moisture front. In effect, a lower k_r for a given ψ causes more of the moisture entering a

finite element to be allotted to increased storage, and less to be passed through as moisture flow. This results in a steeper saturation profile at a given time (Fig. 4.15).

Modification of the ψ vs. S curve A to C in Fig. 4.13 will have a minor effect, if the k_r vs. ψ curve is unchanged. For actual soil, of course, this would not be the case. As reported by Hanks and Bowers [1963] , effects of such modifications seem to be more pronounced for changes in the region of the curves near saturation. The results from the numerical model confirm this, especially when infiltration curves are the object.

In using the relations of Brooks and Corey [1964] to describe unsaturated hydraulic properties of the soil, it is important to recognize the sensitivity of the soil curves to errors in the parameters. In measuring the moisture-tension curves for the Poudre sand, it appeared that an error in the estimation of S_r was counterbalanced by the accompanying displacement of the S_e vs. ψ curve, so that the intercept p_b was not very sensitive to this estimate. The exponents λ and ε , however, are functions of S_r because they are functions of the slope of the logarithmic plot, and when k_r is evaluated by use of equation (2.17), these small errors can be significant. It is fortuitous that such errors will be greatest in the regions where k_r is smallest, and least effective in the solution for infiltration rates. When a soil exhibits a very steep slope in the saturation-tension relationship, however, the exponent ε becomes quite large, and the error in k_r can be significant.

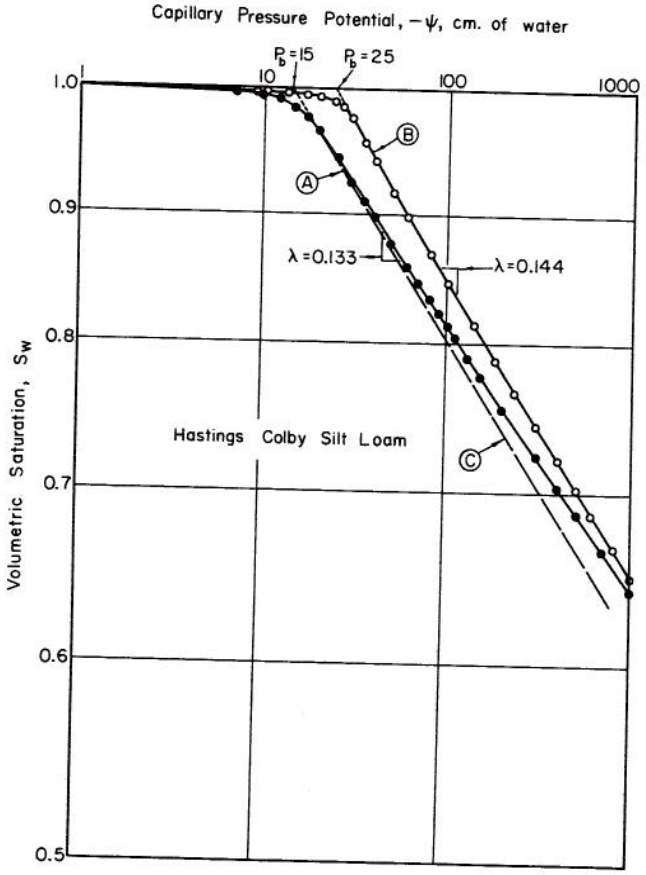

Fig. 4.13. Saturation - capillary pressure relations for two similar soils.

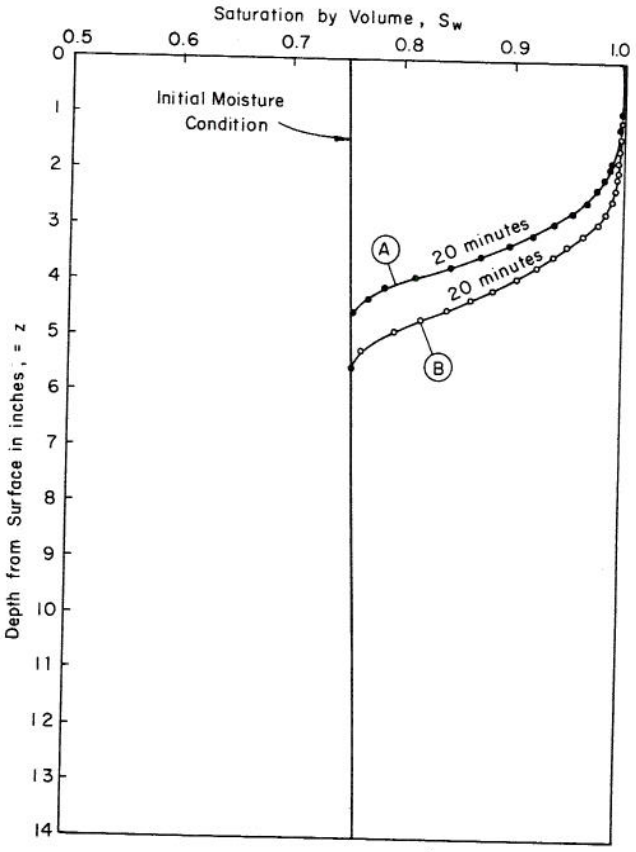

Fig. 4.14. Effect of shift in the saturation-capillary pressure relation on the moisture saturation profile.

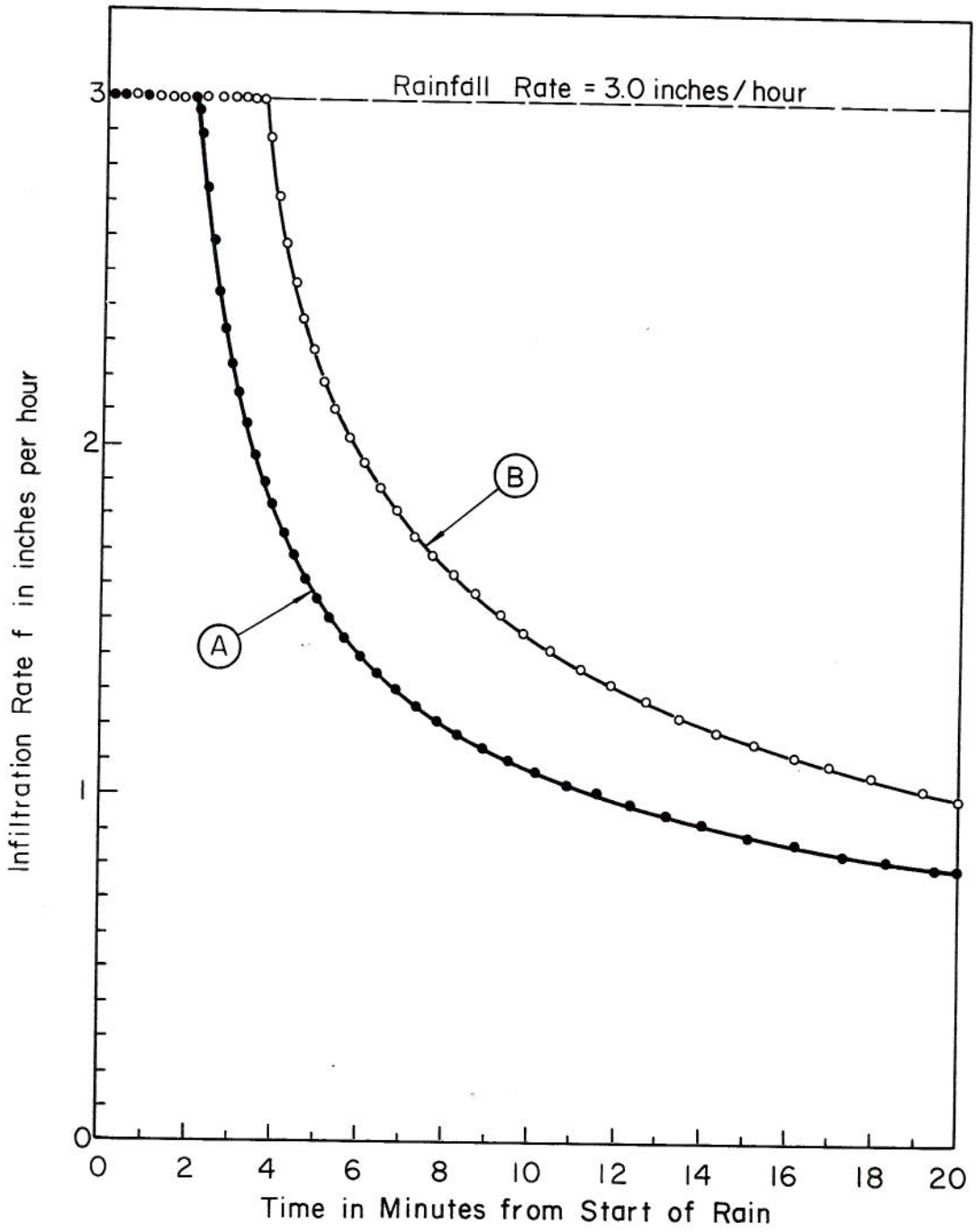

Fig. 4.15. Effect of shift in the moisture-tension relation on the computed infiltration rate.

CHAPTER V

LABORATORY AND FIELD EXPERIMENTS

No matter how sound the physical basis for a mathematical model, one always wishes to compare its performance with careful observations of the process being modelled. Considering the threat of the many types of experimental error, as well as the simplifications involved in formulating the model, this is admittedly a hazardous undertaking. Nevertheless, one may gain useful insight into the sensitivity of the model to measured input parameters, as well as its general efficiency and applicability as a research tool.

Simulation of a Laboratory-Scale Infiltrating Watershed

In order to determine concurrently the performance of the numerical model in predicting soil water movement and surface runoff processes, a laboratory scale soil flume was modified to create a prototype scale infiltrating slope.

Description of the Soil Flume. The soil flume, shown schematically in Fig. 5.1, consists of two parallel reinforced plates, 4 feet high by 40 feet long, containing a 2-inch thickness of soil. The side plates are made of 4- x 4-foot, 3/4 inch thick panels, held by reinforcing angles. The central four panels are of plexiglass, and three on each end are of aluminum.

The ends of the flume are porous and consist of a fiberglass filter supported by a copper screen, all encased in a channeled end plate to collect seepage flow. The bottom is of heavy steel to insure rigidity. The slope of the flume may be changed by raising one end with a permanently mounted hydraulic lift.

The flume was originally designed for studies of saturated groundwater flow, employing point sources of fluid. To prevent algal growth, the fluid used is a light oil resembling refined kerosene, used in the petroleum industry for testing the hydraulic properties of test cores. It is sold by the Phillips Petroleum Company and is referred to as "Soltrol"[1/] or "Phillips Core Test Fluid." The fluid properties are listed in Table 5.1.

Table 5.1

Fluid Properties of "Soltrol"

	Temperature, °C				
	21	22	23	24	25
Density gm./cc.	.7576	.7569	.7562	.7556	.7549
Kinematic viscosity cm.^{2}/sec. x 10^2	2.047	2.011	1.975	1.941	1.907

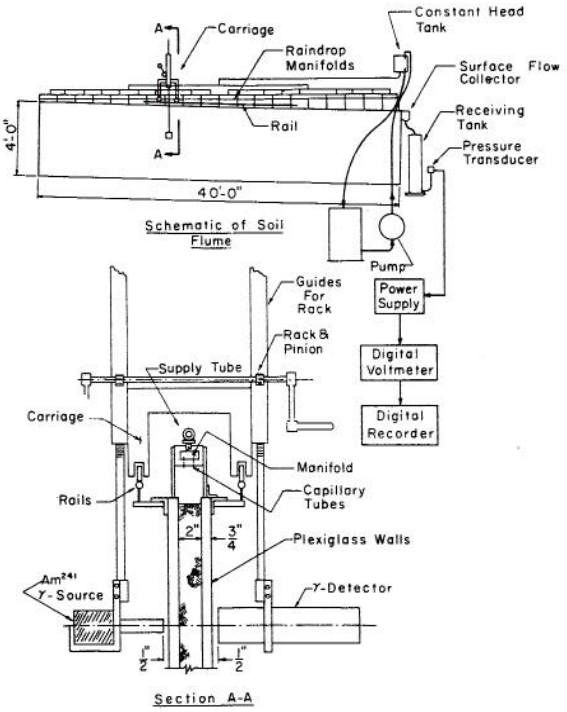

Fig. 5.1. General schematic of the laboratory soil flume and instrumentation for studying watershed response.

For use in studies of flow in porous media, the remaining important property of this fluid is its surface tension, or its capillary properties. This was determined by a laboratory measurement of saturation vs. fluid tension for the soil used in the flume. [See Smith (1970)].

The soil used is a locally obtained river-deposited sand, known as Poudre fine sand. Previous investigators placed the soil in the flume in thin layers. Although care was taken in placing the sand, uniform density was not achieved.

The Rainfall Simulation Apparatus. To allow the flume to be used to study the effectiveness of the mathematical model, equipment was added to (a) generate uniform fluid inputs at the surface, (b) measure the vertical movement of moisture through the soil, and (c) measure the rate of surface runoff, or the watershed hydrograph.

1/ Manufactured by Phillips Petroleum Company, Bartlesville, Oklahoma. Trade names and company names used in this paper are included for information only and do not constitute endorsement by the U. S. Department of Agriculture.

To provide a simulated source of rainfall, drop-producing manifolds were constructed similar to those used by Chow and Harbaugh [1965] at the University of Illinois. A diagram of one of these 20 units constructed is shown in Fig. 5.2, and an installed unit is shown in Fig. 5.3. The entire 40-foot surface was covered with these units, which were supplied with fluid from a constant head tank. The supply line was split sequentially so that pressure was nearly uniform in the manifolds. Drops were produced through the capillary tubes on the lower face of the manifold at a rate determined by the pressure in the manifold, from zero up to a maximum pressure. Above this pressure, depending upon the size of capillary tube, the drops become a continuous stream.

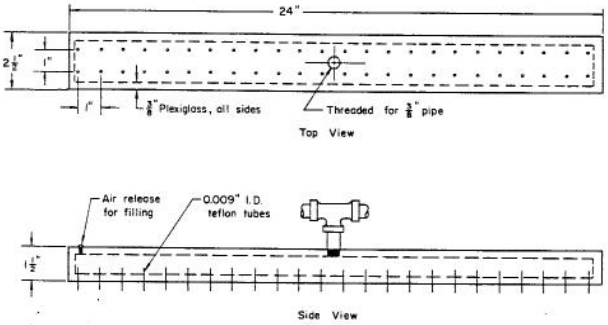

Fig. 5.2. Plan of a raindrop producing manifold unit.

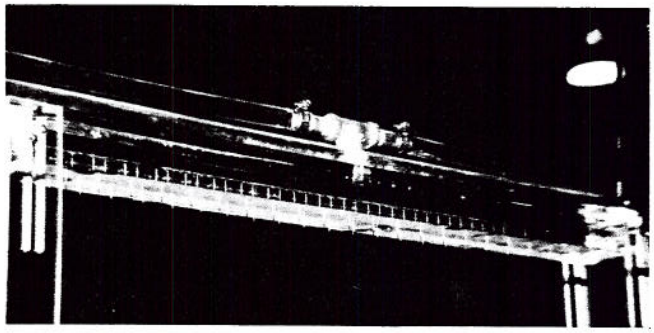

Fig. 5.3. Drop producing unit mounted on top of flume.

The soil surface was covered with 2-inch medical bandage gauze to prevent raindrop erosion. A surface runoff collector, with a sill flush with the soil surface, was mounted at the lower end of the flume. The runoff volume at any time was measured by collecting all runoff in a calibrated tank and sensing the fluid level with a pressure transducer. Pressures were converted to voltages, which were read at 5-second intervals and printed by a paper tape printer. Voltages were converted to volume of fluid by use of the known calibration of the collecting tank, and the differential of the volume over each 5-second interval was the rate of flow for that interval. The runoff measuring equipment and constant head tank are pictured in Fig. 5.4.

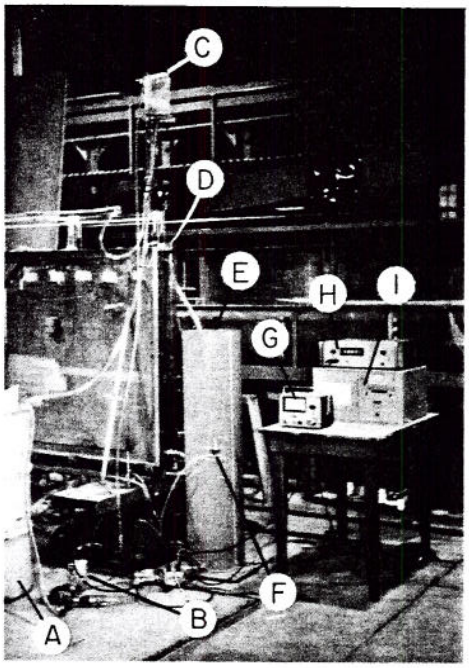

A-Soltrol barrel

B-Pump

C-Constant head tank

D-Collector for surface flow

E-Surface flow measuring tank

F-Pressure transducer

G-Transducer power supply

H-Digital voltmeter

I-Paper tape printout

Fig. 5.4. Lower end of flume, showing equipment for measuring surface runoff.

The Measurement of Soil Moisture Movement. To follow the movement of the infiltrating fluid down into the flume, a carriage assembly was designed and constructed, which would allow use of γ-ray attenuation to measure local saturation of the soil. This carriage is depicted in Fig. 5.1, and the source side and detector side of the unit are pictured in Figs. 5.5 and 5.6, respectively. The theory by which soil moisture is determined from gamma-attenuation theory is presented briefly in Appendix A.

The carriage assembly was mounted on rails over the section of the flume with plexiglass walls. The source and detector were mounted colinearly (or nearly so) on individual racks that moved vertically in square machined sleeves. The racks were moved by pinions on a common shaft, turned by a hand crank, as shown in Fig. 5.1. A friction clamp held the units at any vertical position.

Experimental Procedure. The first step in simulating the watershed response of this laboratory soil flume was to determine the relation between the pressure at the constant head tank and the rate of rainfall on the surface. This was accomplished by installing a collector channel with a semi-circular cross section in the flume over the soil to collect all the rainfall. Rainfall rates computed by means of steady runoff rates were measured for several elevations of the constant-level tank. The relation of rainfall rate to fluid level is shown in Fig. 5.7.

Experiments were performed using a rainfall rate roughly two to three times the saturated conductivity of the soil. Rainfalls of 15 minutes were used, and both dry and moist initial conditions were used. Because a minimum of 30 seconds was necessary to count the gamma rays through the soil, instantaneous

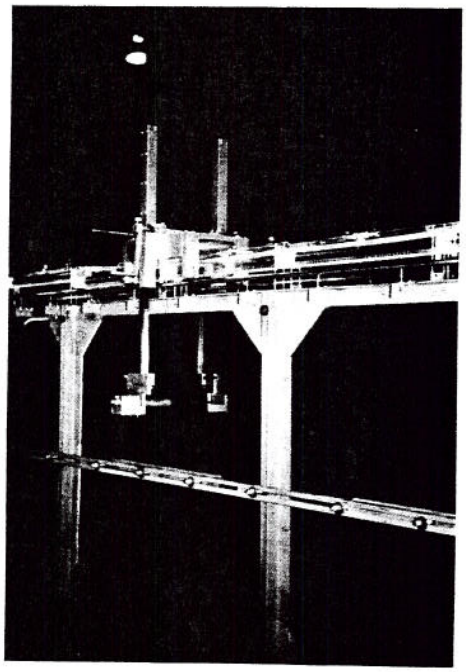

Fig. 5.5. Gamma-ray source and carriage on soil flume.

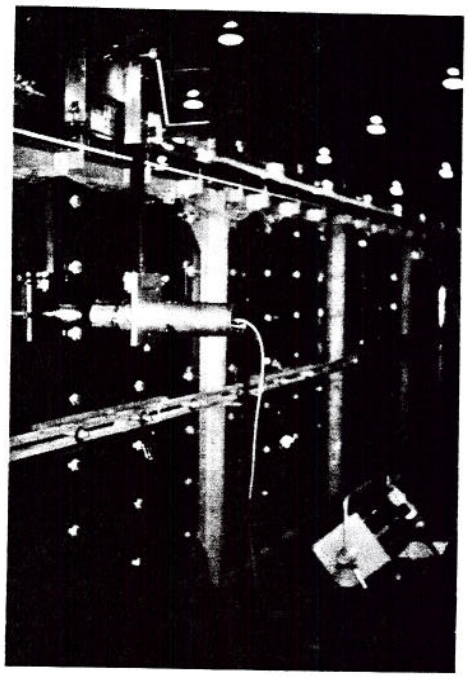

Fig. 5.6. Gamma-ray counter unit. Picture shows opposite side from Fig. 5.5.

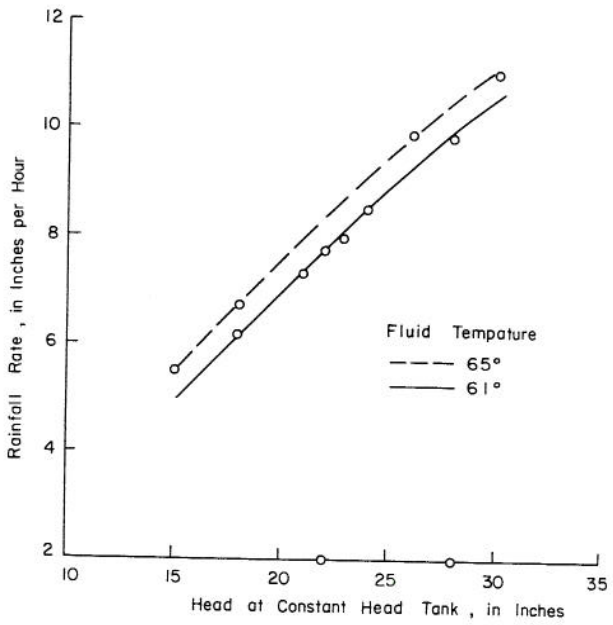

Fig. 5.7. Relation between rainfall rate and fluid head at the constant level tank.

soil profiles during rainfall could not be obtained. However, the location of the steep part of the saturation profile was obtained quite accurately at several stages for each experimental "event."

Numerical Simulation. Laboratory measurement of the unsaturated hydraulic properties of the soil and the saturated conductivity and porosity provided the necessary input to the mathematical model for soil moisture movement. These properties were determined for the two extreme bulk densities found in the flume, and the properties of an intermediate density were interpolated from the other data. The map of bulk densities determined by gamma-counting as described above was then interpreted in terms of gross layers corresponding to these three densities, and these layers were used in the numerical model. For the surface flow portion of the model, the slope and length were measurable, and roughness was a fitted parameter. The exponent m was determined by use of equations (3.4) and (3.22) since $Q(t)$ was measured at the end of the flume.

Simulation of a Field Plot Watershed

Modeling a field plot watershed provides an experiment significantly different from the laboratory prototype scale simulation. The watershed slope, surface roughness, and soil properties are not the same at each point, and the rainfall and runoff data available are not as accurate as laboratory measurements.

The purpose of simulating the runoff response of a field plot watershed to rainfall is to determine the sensitivity of the simulation model to the above-mentioned inhomogeneities, and to see if approximate information concerning the unsaturated hydraulic properties of the soil may be used to predict the observed runoff within acceptable limits of error.

Selection of a Field Plot. The data available on hydraulic properties of the soils came from an Agricultural Research Service publication listing results of extensive sampling of ARS watersheds [Holtan, et. al., 1968]. From these watersheds, it was desired to select a field plot with soil as uniform as possible. Furthermore, the plot should be as near as possible to a point from which sampled soil data were available. It was also desirable to avoid clay soils which would be subject to cracking.

The site chosen was field plot 56-H in the Hastings, Nebraska, Watershed. The soil type is Colby silt loam and the plot is unfurrowed natural pasture covered with native grasses. Plot 56-H is next to a continuously recording rain gauge, and the contour maps available for this area indicate quite uniform overall slope. A map of the watershed site is given in Fig. 5.8. Data were taken at this site from 1939 to 1945.

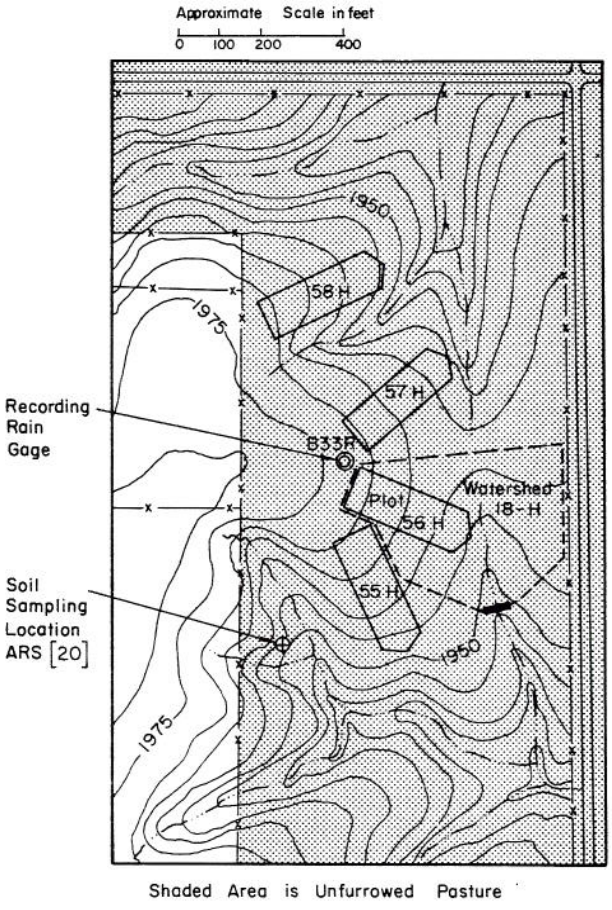

Fig. 5.8. Map of a portion of the Hastings, Nebraska experimental watershed, showing pasture plot 56-H.

Derivation of Soil Properties. The data from the ARS on the watershed soils include tension plate desaturation moisture-tension data for each soil layer in the profile, at 0.10, 0.30, 0.6, 1.0, 3.0 and 15.0 bars tension, porosities at 0.30 bars and oven-dry condition, and saturated conductivity. These data were taken on undisturbed "clods" of the material in most cases.

To obtain useful curves from these data, the few data points for S were used to derive λ in equation (2.18), by logarithmic plotting of S_e vs. ψ. In most cases a straight line fit could be obtained. The region near saturation where the curvature is negative, neglected by the Brooks and Corey formula, had to be fitted by eye. Furthermore, an imbibition curve had to be extrapolated from the desaturation curve by using a logarithmically parallel line. The process proceeds as follows: the moisture percentages by weight given in the data for each soil layer are converted to saturation by volume. This employs the porosity relation, equation (4.7), developed from the two porosities given. In several cases, the data were in error, since volume saturation at 0.1 bar tension was considerably greater than the porosity at 0.3 bar. Some judgment is necessary in conversion of these data, because values given are certainly not as accurate as the number of decimal places given. The point ϕ_{min} must be chosen arbitrarily, and was taken to be ϕ at 2.0 bars tension.

The volume saturation is computed as

$$S = \frac{W}{100} \rho_s (1 - \phi) \qquad (5.1)$$

where W = water content in % dry weight

ρ_s = solid density of soil = 2.65 .

Relative saturation is then computed by the relation

$$S_e = \frac{S - S_r}{1 - S_r}$$

where S_r is residual saturation, a value chosen to make the S_e vs. ψ curve linear on a logarithmic plot. This parameter was proposed by Brooks and Corey [1964] simply as a fitting parameter.

Having estimated λ from the log S vs. log ψ, curve, the exponent describing the relative permeability curve is derived from equation (2.19):

$$\eta = \varepsilon\lambda = 2 + 3\lambda$$

where η = slope of the permeability-tension curve in logarithmic plotting. Relative permeability is then given by $k_r = \left[\frac{P_b}{\psi}\right]^{\eta}$.

Soil curves for Colby silt loam derived in this manner are given in Figs. 5.9 and 5.10.

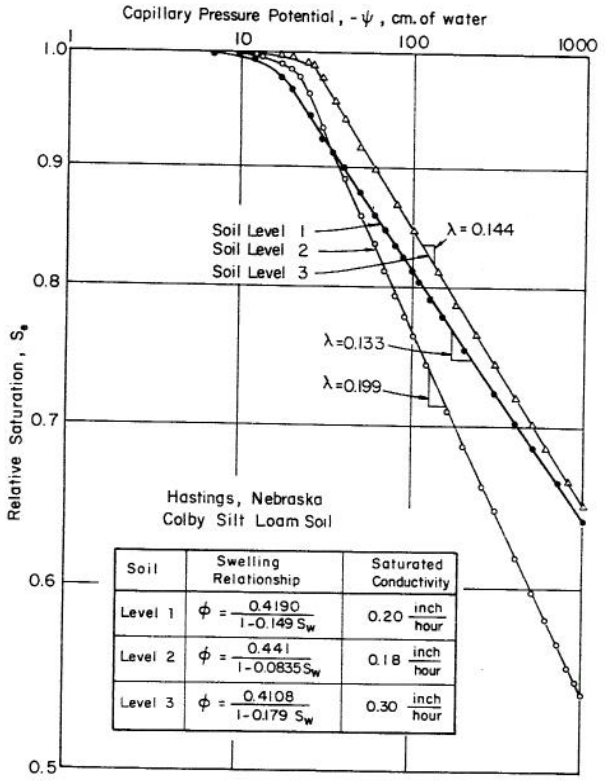

Fig. 5.9. Saturation-capillary pressure relation derived for Colby silt loam.

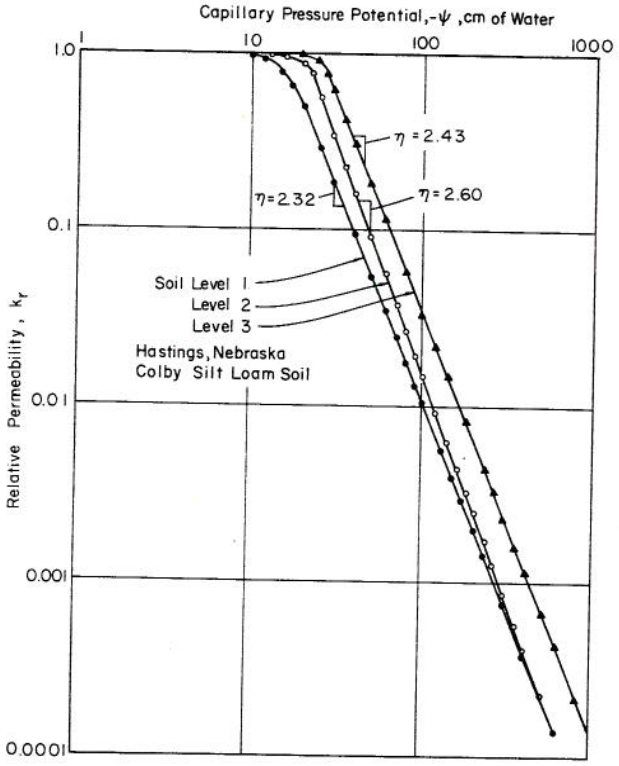

Fig. 5.10. Relative permeability-capillary pressure relation derived for Colby silt loam.

Selection of a Storm for Simulation. Detailed rainfall and runoff data on a 1-minute incremental basis were obtained for most of the storms producing runoff on each subwatershed. Soil moisture at 1-foot increments to a depth of 4 feet was measured by volumetric sampling twice each year.

Storms were selected from these data on the basis of closeness in time to the date of soil moisture sampling, and simplicity of the rainfall pattern. Unfortunately, no storm met both criteria well. Either initial moisture was estimated from descriptions such as "dry" or "moist", or the storm was double peaked, and sufficient moisture redistribution took place during the storm to make the use of the imbibition soil relations invalid, due to hysteresis (Chapter II).

Storms were selected as a compromise between desired knowledge of initial conditions, and simplicity of rainfall pattern. It appears, however, that no simple storms occur in southern Nebraska.

CHAPTER VI

RESULTS AND DISCUSSION

Results of Numerical Simulation of the Laboratory Soil Flume

To model the soil in the laboratory flume, it was first necessary to obtain a map of the variations in soil density, to identify layers of soil for the mathematical model. The method used was described in Chapter V. Results of density measurements are presented in Fig. 6.1. These data show that the density scatters considerably, as would be expected considering the method used to fill the flume. In general, the density increases with depth, as would also be expected, probably as a result of overburden pressure.

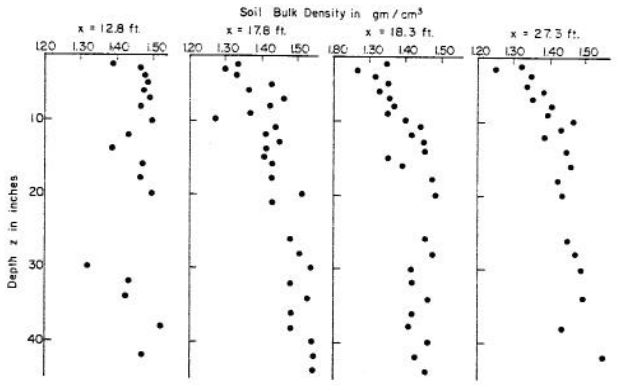

Fig. 6.1. Soil bulk densities at four sections of the soil flume as determined by gamma-attenuation.

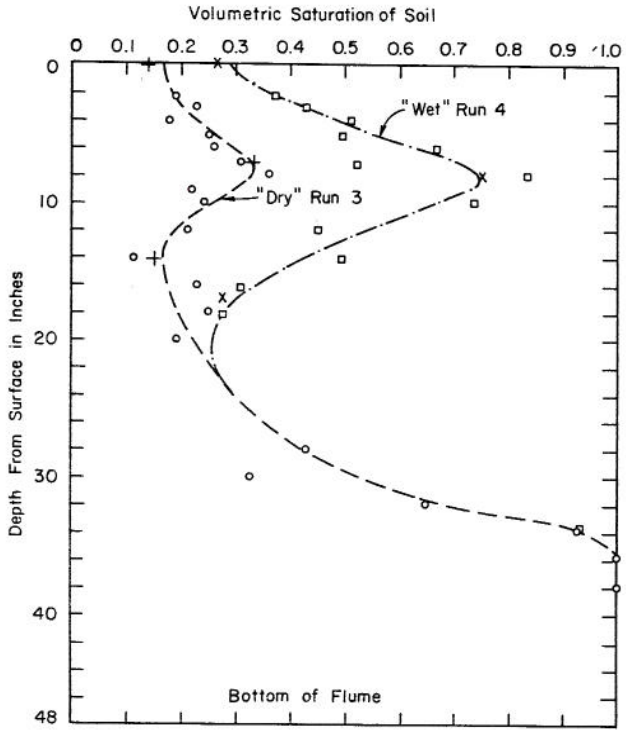

Fig. 6.2. Initial moisture conditions for the wet and dry runs as determined by gamma-attenuation.

Experimental Results. Five experimental runs were made on the laboratory flume. Two types of initial condition were used: the first was a relatively dry condition where the flume had been unused for several weeks, and the water table was at about the 42-inch depth. The second condition was found by repeating a rainfall only a few hours after the dry condition rainfall experiment had been run. Initial conditions as recorded by the gamma-attenuation equipment for a typical dry and wet run are shown in Fig. 6.2, taken at the section X - 18.3 feet, measured from the lower end of the flume.

The results of laboratory determination of the unsaturated hydraulic properties of the soil are shown in Figs. 6.3 and 6.4. Due to repeated failures of laboratory equipment, the curve for k_r vs. S at ρ_b = 1.25 was not completely determined in the laboratory. Good values for k_r at $\psi = 0$ were found for this soil, however, which is a most important value for infiltration studies. The missing part of the curve was determined from the laboratory results of the S vs. ψ relation, equation (2.17), and analogy with other laboratory data. Curves for the sand at the intermediate bulk density (ρ_b) were determined by interpolation between the experimentally determined curves. The work of Laliberte [1966] on properties of unconsolidated media indicates that K_s is a non-linear function of ρ_b, with K_s for an intermediate ρ_b being nearer the value of the higher ρ_b. This was used as a guide in estimating K_s for ρ_b = 1.36. Curves for ψ vs. S vs. k_r were obtained by linear interpolation, in the absence of evidence to show the relationship of these values to ρ_b.

The soil density variation as shown in Fig. 6.1 was approximated by using layers composed of the three bulk densities for which the properties had been derived as described above. The initial saturation profile was approximated from the data shown in Fig. 6.2. These soil and saturation conditions derived for the mathematical simulation are shown in Fig. 6.5.

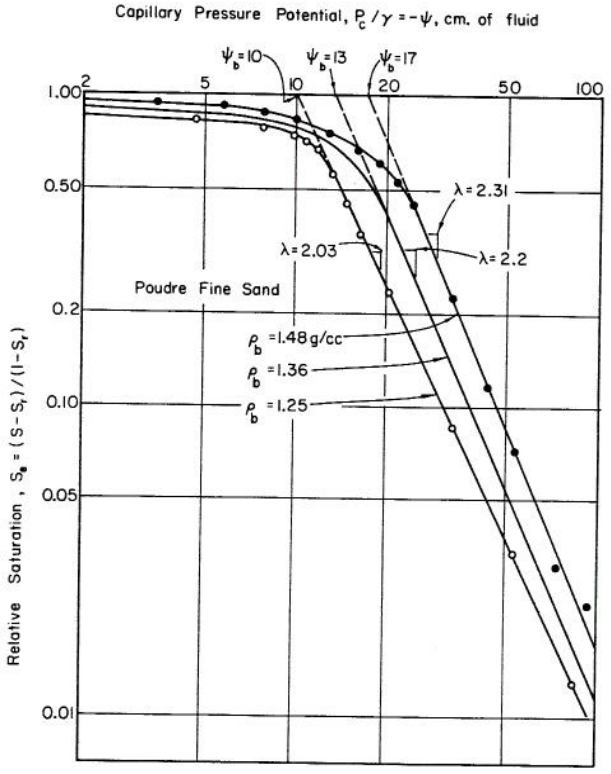

Fig. 6.3. Saturation-capillary pressure imbibition relations for three bulk densities of Poudre fine sand.

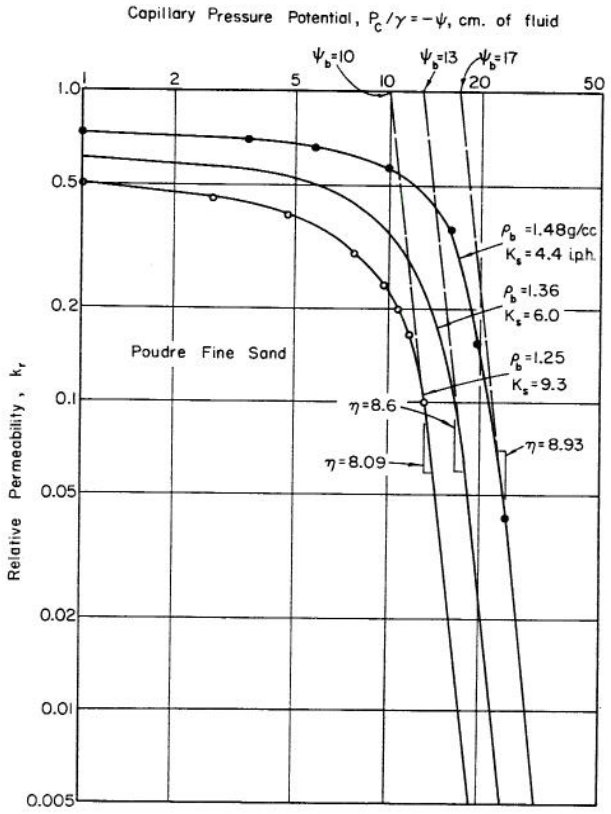

Fig. 6.4. Relative permeability-capillary pressure imbibition relations for three bulk densities of Poudre fine sand.

Watershed hydrographs resulting from laboratory experiments and from the numerical simulations are shown in Figs. 6.6 and 6.7. The corresponding data for moisture profiles in the soil are presented in Figs. 6.8 and 6.9.

Due to the construction of the soil flume, data for density and saturation of the upper 1 1/2 inches of the soil could not be obtained with the γ-attenuation equipment. As a result, it was necessary to estimate soil density and saturation at the surface layer. The scatter of values in the data for initial conditions also left some room for interpretation.

The relationship between surface depth and quantity of surface flow involves determination of two other important parameters. The exponent m and coefficient C in equation (3.4) can be estimated from equation (3.4) and (3.22) using the experimental surface hydrograph, and the rainfall excess curve. Using the simulated excess curve and the experimental runoff hydrograph in equation (3.4) yields a value of m very close to 2 and a value of 4×10^5 for C' , as in Fig. 6.10. Thus a laminar flow relation was assumed, and used in the simulation shown in Figs. 6.6 and 6.7. The roughness coefficient indicated by Fig. 6.10 can be compared with a theoretical value as shown below.

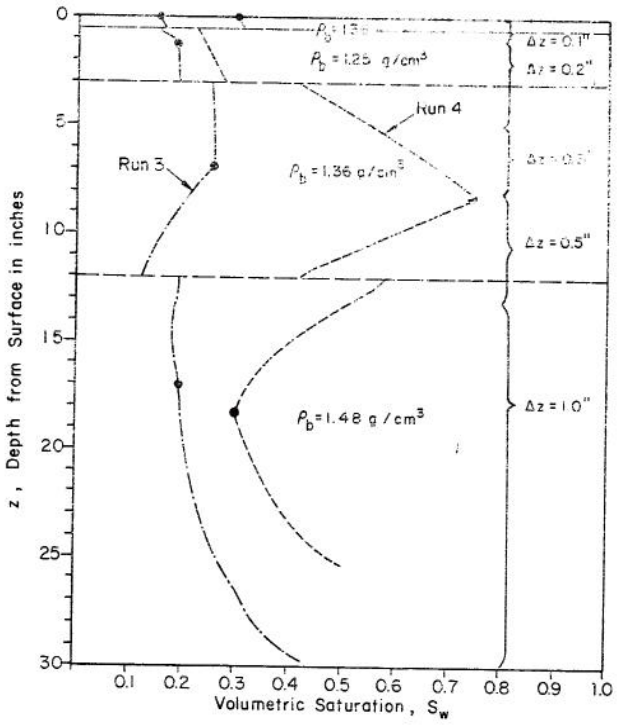

Fig. 6.5. Simulated density layers and initial conditions for the laboratory experiments.

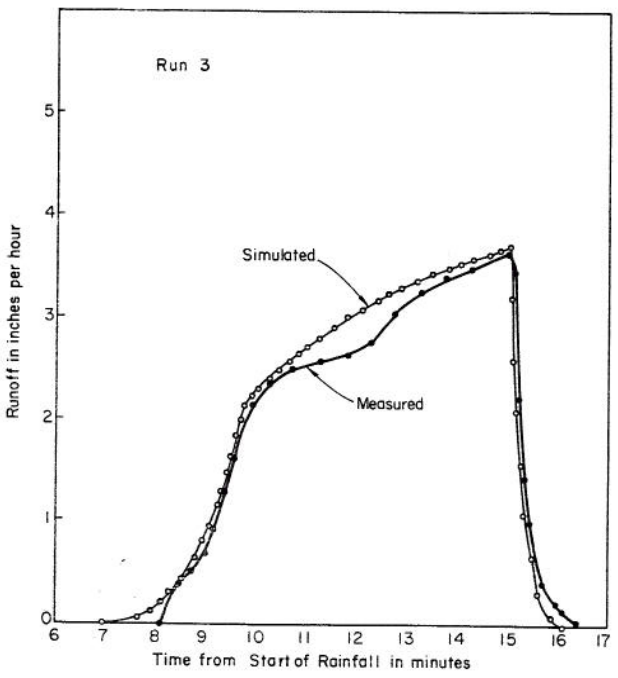

Fig. 6.6. Measured and simulated hydrographs for run 3 with dry initial conditions.

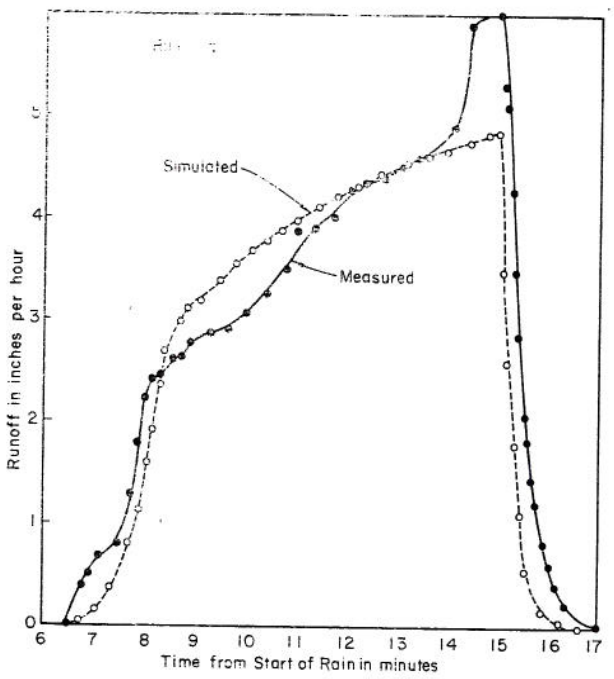

Fig. 6.7. Measured and simulated hydrographs for run 4 with moist initial conditions.

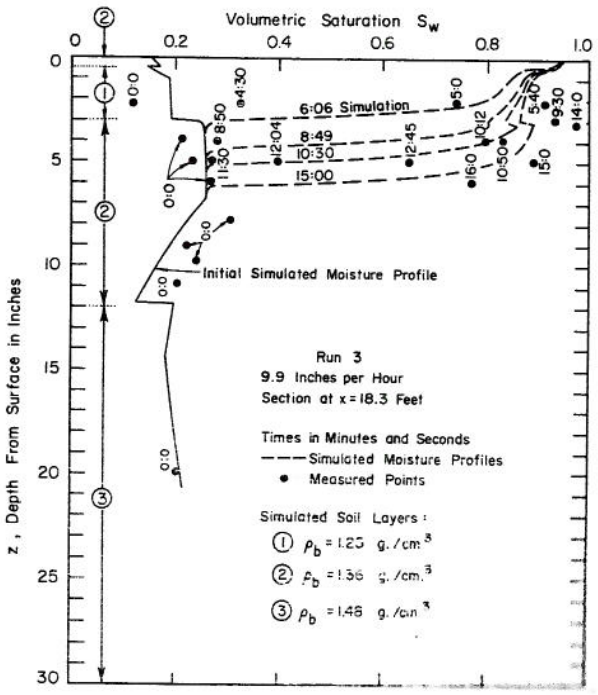

Fig. 6.8. Measured and simulated moisture profiles during run 3.

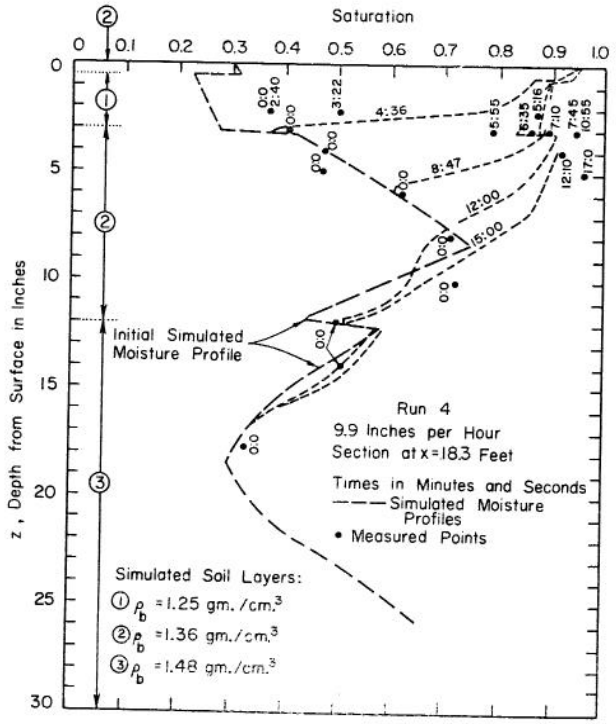

Fig. 6.9. Measured and simulated moisture profiles during run 4.

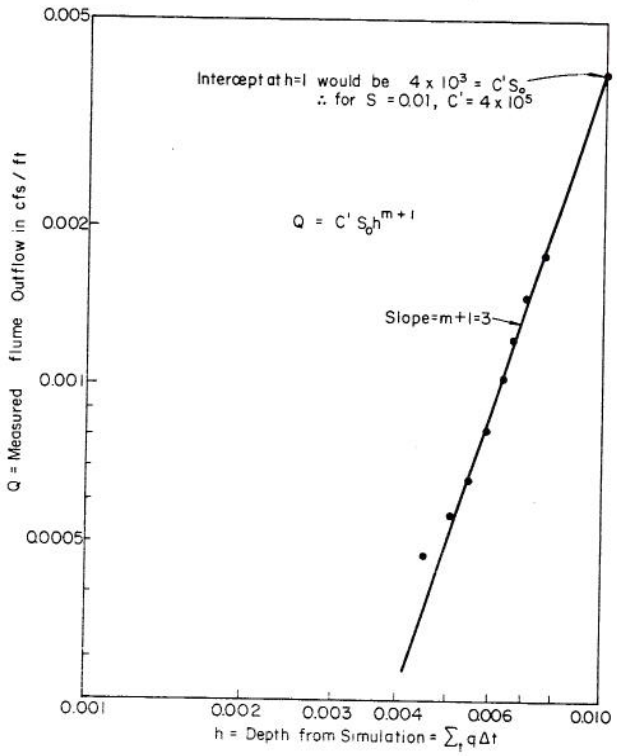

Fig. 6.10. Plotting of computed depth vs. measured outflow Q(t) to estimate m and C' for equation (3.4).

For a laminar flow relationship,

$$q = C'Sh^3$$

where C' is analogous to, but quite different from the Chezy resistance coefficient. The Darcy-Weisbach friction factor f is theoretically inversely proportional to Reynolds number R_n in the laminar flow range:

$$f = \frac{k_f}{R_n} \qquad (6.1)$$

where k_f is 24 for the theoretical smooth case. It can be shown that C' is related to k_f as follows:

$$C' = \frac{8g}{k_f \nu} \qquad (6.2)$$

where g = 32.2 = gravitational constant, (ft/sec^2)

ν = kinematic viscosity in ft^2/sec .

When $k_f = 24$, $C' = 5 \times 10^5$.

A value of 4×10^5 was found to fit the laboratory results well, when two infiltrating points, at each end of the flume, were used in the numerical model. Soil densities were sufficiently variable from point to point and data were not available at a sufficient number of points along the flume to justify attempting to model the flume by taking a greater number of infiltrating points.

Comparison between measured and simulated hydrographs consistently showed a more extended recession for the flume data than for the simulation. This disagreement could be caused by either a failure of the surface flow equations to describe surface flow, or failure of the infiltration model to describe infiltration, or perhaps both. For run 4, with wet initial conditions, air compression is a likely cause of the rapid jump in runoff near the end of the rainfall. This model does not account for such air counterflow. A reduction in infiltration due to air pressure gradients could perhaps account for some of the difference in recession characteristics. Bubbles were noticed escaping from the surface during the latter part of the laboratory runs.

The soil moisture profiles from the flume measurements and the corresponding results from the mathematical model, in Figs. 6.8 and 6.9 show a reasonable agreement. The gamma-attenuation method, under the conditions of this experiment, could not be expected to yield data with better accuracy than 5 to 10%. It appears that the mathematical model overestimates the speed of the moisture "front" by approximately 10%.

It should be kept in mind that the simulation assumed a soil varying abruptly at a few layers, and nearly uniform along the plane, whereas in fact changes in the soil density occurred smoothly and on a scale of inches. This fact, along with the uncertainty concerning the true properties of the upper 1 1/2 inches of soil, results in some uncertainty concerning the effective gross soil properties to be used in the simulation model. The recession and the gamma-attenuation data indicate a possibility that runoff is occurring sooner, with the rainfall excess curve rising somewhat more slowly than is predicted by the mathematical model. The surface hydraulic roughness would then be greater, which is reasonable. With the data used, however, the overall agreement of experimental results and mathematical simulation is still quite acceptable.

Results of Experimental Simulation of a Small Watershed Plot

Simulation of experimental watershed plots from Hastings, Nebraska, presented a considerably different problem. For one thing, all soil and hydraulic information was less detailed and accurate than for the laboratory model. Soil imbibition curves had to be estimated from desaturation curves, for which only a few points were available. Two values for saturated conductivity were given by the data source, with a wide difference between them (.18 to .81 inches/hour). Thus saturated conductivity could not be taken as a known parameter. The roughness of the surface was unknown, and the slightly undulating surface was necessarily assumed to be a plane. Furthermore, the initial moisture condition of the storms could only be estimated.

With these limitations, attempts at simulation of plot watershed data are best considered as an exercise in fitting of physical parameters into a theoretical framework. The results were, however, quite encouraging. Fig. 6.11 shows the rainfall pattern for the storm of June 29, 1944, along with the measured and simulated hydrographs. Values for K_s , C' , and initial saturation profiles were fitted by trial. The roughness used for simulation was C' = 900 , which corresponds to the value for turfed surfaces reported by Morgali [op.cit.]. The soil was modelled as a layered system to correspond with the ARS soil sampling data, with layers of 5", 6", and 30", corresponding to the curves shown in Figs. 5.9 and 5.10. Saturated conductivities used for these soils were 0.20, 0.18, and 0.30 inches per hour, respectively. These are also quite reasonable values.

By comparison with the laboratory flume, runoff rates for the storms simulated on the Hastings, Nebraska field plots never came near the equilibrium rate for any of the rainfall pulse rates in the storm. Runoff from the flume was, on the other hand, very close to the rainfall rate minus infiltration rate by the end of the rainfall pulse. As a result, for simulating the plot watershed response, surface roughness becomes a very important parameter in matching peak rates of runoff.

Foster [op.cit], in work on field plots using an algebraic infiltration formula, found that actual recessions were more extended than the prediction. He hypothesized that this may be explained by a limitation of infiltration ability due to confining of the surface water to rivulets. His method was to

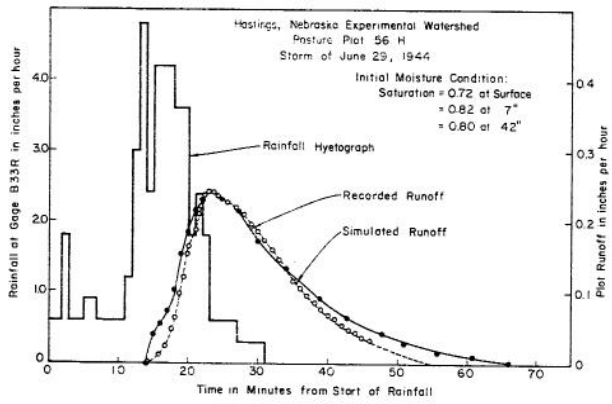

Fig. 6.11. Rainfall pattern, measured and simulated hydrographs for June 29, 1944 storm on Hastings pasture plot 56-H.

reduce the infiltration rate by 75%. It seems reasonable that the microtopography on a field plot would result in a confined area with infiltration opportunity. A very simple formula was used to simulate such effects in this model. Microrelief was assumed to be distributed in elevation such that infiltrating area was linearly distributed between a minimum area when depth of water was near zero, to the complete covering of the watershed when the surface water depth became greater than some maximum value. No doubt, a much more physically based model could be derived to simulate this and other surface effects. Use of this simple surface relief model improved the agreement of recessions for this watershed.

To test the validity of parameters C' and K_s fitted for this storm, the same values were applied to another storm, for June 5, 1945, with initial soil moisture distribution as the only fitting parameter. The results for this storm, compared with the recorded hydrograph are shown in Fig. 6.12.

Each of these storms was described as occurring on a "moist" soil condition, and indeed the fitted soil saturations used for the results of Figs. 6.11 and 6.12 are quite similar. It should be pointed out that for the measured hydrographs, the coincidence of timing of the rainfall rates and runoff data could be as much as five minutes in error, from experience with the clocks used in such instrumentation.

The parameters developed for the two storms above were also applied to a storm for which initial soil saturation data was measured a few days prior to the storm. This storm, shown in Fig. 6.13, has a double peak, and the soil curves used which only describe imbibition should not be able to model well the redistribution of moisture between the two rainfall peaks. The excellent agreement for this storm is in part due to a fortuitous estimation of initial soil moisture, based on data from five days previous. Also, it appears from these three storms that recessions are modelled most accurately for storms with little runoff, and least accurately when runoff is high. This could be connected with misestimation of long period infiltration, and effects of air counterflow. It could also be connected with the actual hydraulic effect of the grass as a roughness element,

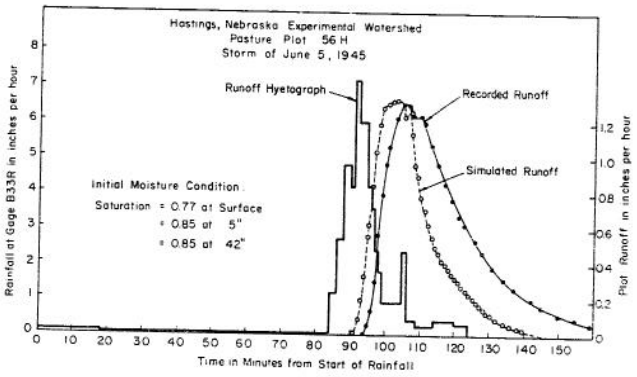

Fig. 6.12. Rainfall pattern, measured and simulated hydrographs for June 5, 1945 storm on Hastings pasture plot 56-H.

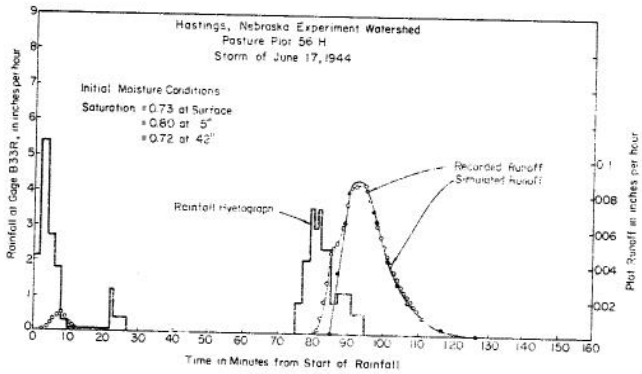

Fig. 6.13. Rainfall pattern, measured and simulated hydrographs for June 17, 1944 storm on Hastings pasture plot 56-H.

or surface seal development when fine material is being transported in the infiltrating surface water.

Computer running time for these simulations is dependent on the curvature of the soil moisture-tension curves, the rate of imposed rainfall, and the size of Δz increments. For these simulations, the CDC 6400 computer used approximately one second for each minute of simulated storm, and required approximately $70{,}000_8$ core storage.

CHAPTER VII

CONCLUSIONS AND RECOMMENDATIONS

The response of a watershed to rainfall is a very complex natural process. No theoretical model of a natural watershed can conceivably be made which could account for all the variables and their interrelationships that affect the runoff process. On the other hand, no model which is sufficiently simple to be a general engineering tool can hope to model well the result of all these complexities. The objective of model formulation is to make simplifying assumptions so the model is not unwieldy and yet retains the most important characteristics of the physical system.

This study has adopted sufficient simplifying assumptions so that current theories of soil water movement and watershed hydraulics could be combined into a mathematical model of the rainfall-runoff process on small elementary watersheds.

Conclusions. The partial differential equation of one-phase soil moisture movement was solved numerically with the purpose of describing the dependent upper boundary conditions governing infiltration. It was shown that this solution may be obtained with sufficient efficiency and preservation of material continuity to provide a description of infiltration rate as a smoothly varying function of time in agreement with the shape and asymptotic nature of the results of infiltrometer studies. The solutions were found to be sensitive to the size of finite difference elements and to other solution parameters. The results agree in general with previous studies of numerical sensitivity.

It was then demonstrated that this infiltration model may be combined with the kinematic equation of overland flow, with interacting boundary conditions at the soil surface, to provide a mathematical model of the generation of overland flow from rainfall on an infiltrating surface.

For the case where the necessary hydraulic relationships for the unsaturated porous media can be obtained, this model can accurately describe the performance of a relatively simple infiltrating watershed when rainfall occurs. The accuracy of such a prediction for more complex watersheds will necessarily depend on obtaining reliable data for the effective average hydraulic properties of the soil and watershed surface for definable regions within the watershed.

For the case where soil properties are subject to large errors or must be estimated, such a model can provide a theoretical framework for a good description of the watershed response, in which system parameters with physical significance, such as effective saturated conductivity and surface roughness, may be obtained by comparison with experimental data.

Recommendations. The ideal experimental procedure for evaluation of the model developed in this study would be to first test its performance in comparison with the simplest case. As data were obtained from the soil flume used in this work, it became apparent that the soil section in the laboratory flume was a complex rather than a simple case, where soil properties varied significantly in both horizontal and vertical directions. A soil flume in which soil has been placed in a controlled and uniform manner should be used to test this mathematical model.

Many improvements could be made in the facilities for measuring soil moisture movement, which could better evaluate the agreement between theory and experiment. A flume for this purpose should have facilities which allow measurement of conditions near the surface, which appear to be very important in infiltration. Other improvements in laboratory equipment should be made to allow faster determination of point saturation by using a more active or stronger radioactive source, and designing equipment to move more quickly in a vertical direction. The flume should be more uniform in thickness, and should have better facilities for studying unsaturated flow specifically, including control and measurement of air escape, or air compression.

It is not at all certain that the relationship of equation (6.1) describes the true hydraulic resistance of the surface, especially in view of the energy input of the raindrops. To adequately study the role of infiltration, the surface should be made impervious, and the surface hydraulics studied independently. In many cases, the watershed hydraulics may follow a laminar flow relation for part of the hydrograph, a turbulent relation for another, and exhibit transitional characteristics between these periods. Study of this type is currently in progress at Colorado State University, employing a prototype scale watershed, and a mathematical model for runoff on an impervious watershed [Kibler and Woolhiser, 1970].

A mathematical infiltration model could be based on equations (2.14) and (2.15) which would include a model for flow of the air phase. Although this should improve the accuracy of the theoretical model, it would also make the numerical solution more lengthy, and in terms of computer time, much more expensive. To employ the complete two-phase equations would require data for the relation between air conductivity and water saturation. At present, very little soil data are available which include this information, and far less such data for soils in place on watersheds.

To employ a model such as developed in this study, data collection on experimental watersheds should be oriented toward the hydraulic soil properties important in infiltration, rather than the traditional descriptions of soil chemists and agronomists. The soil analyses should obtain such things as imbibition relations between moisture tension, saturation, and unsaturated conductivity. Field measurements of saturated conductivity are also very important, and progress in remote sensing offers hope that in the future, surface and near surface saturations may be obtainable on a large scale basis. With such physically meaningful data, models employing current knowledge of the physical processes involved may be applied to study the watershed surface response.

LIST OF SYMBOLS

Symbol	Description	Dimension
A	Nonlinear operator matrix	--
a	as subscript - refers to air phase, or locally defined constant	--
a_i	off-diagonal element in matrix A	--
b_i	diagonal element in matrix A	--
C	Chézy roughness coefficient, turbulent flow	$L^{\frac{1}{2}}T^{-1}$
C'	laminar roughness coefficient	$L^{-1}T^{-1}$
C_1	constant of integration	--
c_i	off-diagonal element in matrix A	--
D(θ)	diffusivity	L^2T^{-1}
d	subscripted; thickness of material	L
d_i	element of a diagonal matrix	--
e	base of natural logarithms, or voids ratio = $\phi/(1 - \phi)$	--
F	accumulated infiltration	L
F_o	Froude number	--
f	infiltration rate	LT^{-1}
f_c	minimum f	LT^{-1}
f_e	f at t = ∞	LT^{-1}
f_o	f at t = 0	LT^{-1}
g	gravitational acceleration	LT^{-1}
H_o	normal depth of flow based on Q_o	--
h	depth of water on the surface	L
I	count rate in attenuation measurement	T^{-1}
I_o	base count rate in air	T^{-1}
i	subscript, refers to node number for finite difference grid in length dimension	--
j	superscript, refers to node number for finite difference grid in time dimension	--
K or K_s	conductivity of saturated porous media	LT^{-1}

Symbol	Description	Dimension
k	indicates plane number for cascaded planes, or permeability of porous medium	-- L^2
k_*	kinematic parameter = $S_o L_k / H_o F_o^2$	--
k_f	coefficient in roughness relationship for laminar flow	--
k_r	relative permeability or relative conductivity	--
L	depth to water table	L
L_k	length of plane k	L
M_x	number of grid points used to divide plane k for a finite difference approximation	--
N_z	number of grid points used to divide the soil column for a finite difference approximation	--
n	locally defined constant	--
p	pressure	$ML^{-1}T^{-2}$
p_b	bubbling pressure	$ML^{-1}T^{-2}$
p_c	capillary pressure = $p_a - p_w$	$ML^{-1}T^{-2}$
Q_o	normalizing flow rate per unit width of plane with maximum possible q(x,t)	L^2T^{-1}
Qp	inflow rate at soil surface	LT^{-1}
q(x,t)	local rainfall excess rate	LT^{-1}
Rn	Reynolds number	--
RF	rainfall rate	LT^{-1}
RHS	abbreviation of right side of equation (4.20)	L
rhs_i, r_i	element in vector RHS	L
S	saturation, in general, or locally used constant	--
S_e	relative saturation = $(S - S_r/1 - S_r)$	--
S_f	slope of energy gradient in surface flow	--

LIST OF SYMBOLS (continued)

Symbol	Description	Dimension
S_o	slope of ground surface	--
S_r	residual saturation	--
SL_i	represents $\partial s/\partial \psi$	L^{-1}
$STOR_i$	abbreviation for part of equation (4.13)	LT^{-1}
t	time	T
u	velocity	LT^{-1}
V_b	bulk volume; volume per unit area	L
V_o	velocity at normal depth H_o	LT^{-1}
w	subscript - refers to water or fluid phase	--
W_k	width of plane k	L
X,x	length, usually horizontal	L
Z,z	depth, measured downward from surface	L
α	locally defined constant	--
α_k	coefficient in u-h relationship on plane k	--
β	locally defined constant	--
γ	unit weight	$ML^{-2}T^{-2}$
ε	exponent in empirical relation between S and k_r, or infinitesimal error value	--
η	exponent in empirical relation between ψ and k_r	--
θ	volumetric water content = $S\phi$	--
λ	exponent in empirical relation between ψ and S	--
μ	dynamic viscosity	$ML^{-1}T^{-1}$
μ_b	attenuation coefficient for material b	L^{-1}
ν	kinematic viscosity	L^2T^{-1}
ξ	Lipschitz convergence parameter, $\xi < 1$	--
ρ	density	ML^{-3}
ρ_b	bulk density of porous material	ML^{-3}
ρ_s	solid density of porous material	ML^{-3}
$\rho(B)$	spectral radius of matrix B	--
σ	moisture ratio = $\theta/(1 - \phi)$	--
ϕ	porosity	--
$\phi(\ )$	vector operator	--
ψ	soil water pressure potential = $p_a/\gamma_a - p_w/\gamma_w$	L
ω	locally defined parameter	--

REFERENCES

1. Amorocho, J., "Role of Infiltration in Nonlinear Watershed Analysis Processes," Trans. ASAE, Vol. 10, No. 3, 1967, pp. 396-399,404.

2. Breitenbach, E. A., D. H. Thornau, and H. K. Van Poolen, "The Fluid Flow Simulation Equations," Society of Petroleum Engineers, Paper No. SPE 2020, Symposium on Numerical Simulation of Reservoir Performance, Dallas, Texas, April 22-23, 1968.

3. Brooks, R. H., and A. T. Corey, "Hydraulic Properties of Porous Media," Hydrology Paper No. 3, Colorado State University, March, 1964.

4. Brutsaert, Wilfried, "Probability Laws for Pore-Size Distributions," Soil Science, Vol. 101, No. 2, February, 1966, pp. 85-92.

5. Burman, Robert D., "Plot Runoff using Kinematic Wave Theory and Parameter Optimization," Ph.D. Dissertation, Cornell University, 1969.

6. Childs, E. C., and N. Collis-George, "The Permeability of Porous Materials," Proc. of the Royal Society of London, Series A, Vol. 201, No. 1066, April 26, 1950, pp. 392-405.

7. Chow, Ven Te, and T. E. Harbaugh, "Raindrop Production for Laboratory Watershed Experimentation," Journal of Geophysical Research, Vol. 70, No. 24, December, 1965, pp. 6111-6119.

8. Crawford, N. H., and R. K. Linsley, "Digital Simulation in Hydrology: Stanford Watershed Model IV," Technical Report No. 39, Civil Engineering Department, Stanford University, July, 1966.

9. Fadeev, D. K., and V. N. Fadeeva, Computational Methods of Linear Algebra, W. H. Freeman & Co., San Francisco, 1963.

10. Foster, G. R., L. F. Huggins, and L. D. Meyer, "Simulation of Overland Flow on Short Field Plots," Water Resources Research, Vol. 4, No. 6, December, 1968, pp. 1179-1187.

11. Foster, G. R., "Analysis of Overland Flow on Short Erosion Plots," unpublished M.S. Thesis, Purdue University, Lafayette, Indiana, January 1968.

12. Freeze, R. Allen, "The Mechanism of Natural Ground Water Recharge and Discharge. 1. One-Dimensional, Vertical, Unsteady, Unsaturated Flow above a Recharging or Discharging Ground Water Flow System," Water Resources Research, Vol. 5, No. 1, February, 1969, pp. 153-171.

13. Gill, William R., "Soil Bulk Density Changes Due to Moisture Changes in Soil," Trans. ASAE, Vol. 2, No. 1, 1959, pp. 104-105.

14. Gardner, W. R., "Development of Modern Infiltration Theory and its Application in Hydrology," Trans. ASAE, Vol. 10, No. 3, 1967, pp. 379-381.

15. Gardner, Willard and John A. Widtsoe, "The Movement of Soil Moisture," Soil Science, Vol. 11, January-June, 1921, pp. 215-232.

16. Green, W. H., and G. A. Ampt, "Studies on Soil Physics, Part 1.--The Flow of Air and Water Through Soils," Journal of Ag. Science, Vol. IV, part 1, 1911, pp. 1-24.

17. Green, R. E., R. J. Hanks and W. E. Larson, "Estimates of Field Infiltration by Numerical Solution of the Moisture Flow Equation," Soil Science Soc. of America Proceedings, Vol. 18, No. 1, January-February, 1964, pp. 15-19.

18. Groenevelt, P. H., J. G. deSwart, and J. Cisler, "Water Content Measurement with 60 Kev Gamma Ray Attenuation," Bulletin of the International Association of Scientific Hydrology, Vol. 15, No. 2, June, 1969, pp. 67-69.

19. Hanks, R. J., and S. A. Bowers, "Numerical Solution of the Moisture Flow Equation for Infiltration into Layered Soils," Soil Science Soc. of America Proceedings, Vol. 26, No. 6, November-December, 1962, pp. 530-534.

20. Hanks, R. J., and S. A. Bowers, "Influence of Variations in the Diffusivity-Water Content Relation on Infiltration," Soil Science Soc. of America Proceedings, Vol. 27, No. 3, May-June, 1963, pp. 263-265.

21. Henderson, F. M., "Flood Waves in Prismatic Channels," Journal of the Hydraulics Division, Proc. of the ASCE, Vol. 89, No. HY4, 1963, pp. 39-67.

22. Holtan, H. N., "A Concept for Infiltration Estimates in Watershed Engineering," Agricultural Research Service, ARS 41-51, U.S. Dept. of Agriculture, October, 1961.

23. Holtan, N. H., et.al., "Moisture-Tension Data for Selected Soils on Experimental Watersheds," Agricultural Research Service, ARS 41-144, U.S. Dept. of Agriculture, October, 1968.

24. Holtan, H. N., C. B. England and W. H. Allen, "Hydrologic Capacities of Soils in Watershed Engineering," Proceedings, International Hydrology Symposium, Vol. 1, Fort Collins, Colorado, September 6-8, 1967, pp. 218-226.

25. Horton, R. E., "An Approach Toward Physical Interpretation of Infiltration Capacity," Soil Science Soc. of America, Proceedings, Vol. 5, 1940, pp. 399-417.

26. Ibrahim, H. A., "Hysteresis and Intermittent Vertical Infiltration in Unsaturated Porous Media," Ph.D. Thesis, Cornell University, 1967.

27. Irmay, S., "On the Hydraulic Conductivity of Unsaturated Soils," Trans. American Geophysical Union, Vol. 35, No. 3, June 1954, pp. 463-467.

28. Jackson, Ray D., "Porosity and Soil-Water Diffusivity Relations," Soil Science Soc. of America, Proceedings, Vol. 27, No. 2, March-April, 1963, pp. 123-126.

29. John, R., Lectures on Advanced Numerical Analysis, Gordon and Breach, New York, 1967.

30. Kibler, David F., "A Kinematic Overland Flow Model and its Optimization," Ph.D. Dissertation, Colorado State University, Fort Collins, Colorado, August, 1968.

31. Kibler, David F., and David A. Woolhiser, "The Kinematic Cascade as a Hydrologic Model," Hydrology Paper No. 39, Colorado State University, Fort Collins, Colorado, March, 1970.

32. King, L. G., "Imbibition of Fluids by Porous Solids," Ph.D. Dissertation, Colorado State University, Fort Collins, Colorado, 1964.

33. Klute, Arnold, "A Numerical Method for Solving the Flow Equation for Water in Unsaturated Materials," Soil Science, Vol. 73, No. 2, February, 1952, pp. 105-116.

34. Laliberte, Garland, "Properties of Unsaturated Porous Media," Ph.D. Dissertation, Colorado State University, Fort Collins, Colorado, August, 1966.

35. Lauritzen, C. W., "Apparent Specific Volume and Shrinkage Characteristics of Soil Materials," Soil Science, Vol. 65, January-June, 1948, pp. 155-179.

36. Lauritzen, C. W. and A. J. Stewart, "Soil-Volume Changes and Accompanying Moisture and Pore-Space Relationships," Soil Science Soc. of America, Proceedings, Vol. 6, 1941, pp. 113-116.

37. Laikopoulos, A. C. "Theoretical Solution of the Unsteady Unsaturated Flow Problems in Soils," Bulletin of the International Assoc. of Scientific Hydrology, Vol. X, No. 1, 1965, pp. 5-39.

38. Marshall, R. J., "A Relation Between Permeability and Size Distribution of Pores," Journal of Soil Science, Vol. 9, No. 1, 1958, pp. 1-8.

39. Melrose, James C., "Wettability as Related to Capillary Action in Porous Media," Soc. of Petroleum Engineers Journal, September, 1965, pp. 259-271.

40. Miller, E. E., and R. D. Miller, "Theory of Capillary Flow," Soil Science Soc. of America, Proceedings, Vol. 19, No. 3, July 1955, pp. 267-275.

41. Morgali, James R., "Laminar and Turbulent Overland Flow Hydrographs," Journal of the Hydraulics Division, ASCE, Vol. 96, No. HY2, Proc. Paper 7069, February, 1970, pp. 441-460.

42. Phuc, L. V., "General One-Dimensional Model for Infiltration," M.S. Thesis, Colorado State University, Fort Collins, Colorado, 1969.

43. Philip, J. R., "The Theory of Infiltration: 1. The Infiltration Equation and its Solution," Soil Science, Vol. 83, No. 5, May, 1957, pp. 345-357.

44. Philip, J. R., "The Theory of Infiltration: 4. Sorptivity and Algebraic Infiltration Equations," Soil Science, Vol. 84, No. 3, September, 1957, pp. 257-264.

45. Philip, J. R., "Similarity Hypothesis for Capillary Hysteresis in Porous Materials," Journal of Geophysical Research, Vol. 69, No. 8, April 15, 1964, pp. 1553-1562.

46. Philip, J. R., "Hydrostatics and Hydrodynamics of Swelling Soils," Water Resources Research, Vol. 5, No. 5, October, 1969, pp. 1070-1077.

47. Poulovassilis, A., "Hysteresis of Pore Water, an Application of the Concept of Independent Domain," Soil Science, Vol. 93, No. 6, June, 1962, pp. 405-412.

48. Richards, L. A., "Capillary Conduction of Liquids Through Porous Mediums," Physics, Vol. 1, November, 1931, pp. 318-333.

49. Rubin, J., "Theory of Rainfall Uptake by Soils Initially Drier than their Field Capacity and its Application," Water Resources Research, Vol. 2, No. 4, 1966, pp. 739-749.

50. Rubin, J., and R. Steinhardt, "Soil-Water Relations during Rain Infiltration: I. Theory," Soil Science Soc. of America, Proceedings, Vol. 27, No. 3, May-June, 1963, p. 246-251.

51. Rubin, J., and R. Steinhardt, "Soil-Water Relations during Rain Infiltration: II. Moisture Content Profiles During Rains of Low Intensities," Soil Science Soc. of America, Proceedings, Vol. 28, No. 1, January-February, 1964, pp. 614-615.

52. Rubin, J., and R. Steinhardt, "Soil-Water Relations during Rain Infiltration: III. Water Uptake at Incipient Ponding," Soil Science Soc. of America, Proceedings, Vol. 28, No. 5, September-October, 1964, pp. 614-619.

53. Varga, R. S., Matrix Iterative Analysis, Prentice-Hall, Englewood Cliffs, N. Y., 1962.

54. Whisler, F. D., "The Numerical Analysis of Infiltration, Considering Hysteresis, into a Vertical Soil Column at Equilibrium under Gravity," Ph.D. Dissertation, University of Illinois, 1964.

55. Whisler, F. D., and A. Klute, "The Numerical Analysis of Infiltration, considering Hysteresis into a Vertical Soil Column at Equilibrium under Gravity," Soil Science Soc. of America, Proceedings, Vol. 29, No. 5, September-October, 1965, pp. 489-495.

56. White, N. F., "The Desaturation of Porous Materials," Ph.D. Dissertation, Colorado State University, Fort Collins, Colorado, June, 1968.

57. Wooding, R. A., "A Hydraulic Model for the Catchment-Stream Problem. I. Kinematic-Wave Theory," Journal of Hydrology, Vol. 3, Nos. 3/4, 1965, pp. 254-267.

58. Woolhiser, D. A., and J. A. Liggett, "Unsteady, One-Dimensional Flow over a Plane-The Rising Hydrograph," Water Resources Research, Vol. 3, No. 3, July, 1967. pp. 753-771.

59. Woolhiser, D. A., "Overland Flow on a Converging Surface," Trans. ASAE, Vol. 12, No. 4, 1969, pp. 460-462.

APPENDIX A

Theory of Gamma-Attenuation for Soil Moisture Measurement.

According to Beer's law, attenuation of a parallel beam of gamma rays by a given material is an exponential function of the thickness of the material:

$$I = I_o e^{-\mu_a d_a} \quad , \qquad (A.1)$$

where μ_a is the attenuation coefficient for material a

d_a is the thickness of material a

I_o is the intensity of gamma radiation in counts per minute in the absence of material a

I is the count rate after the beam has passed through the material.

For the case where the beam passes through several materials between source and detector, the attenuation is exponentially additive, that is

$$I = I_o e^{-\mu_a d_a - \mu_b d_b - \mu_c d_c}$$

for three materials a, b, and c.

To use this relation to measure soil moisture saturation, the attenuation coefficients for all the materials must be known. If the soil thickness through which the beam passes is known, the porosity will measure the proportion of this thickness which is pore space--either air or fluid. Thus a given count rate will indicate the thickness of fluid if all other thicknesses and all attenuation coefficients are known. This may be expressed as

$$I = I_o e^{-\mu_w d_w - \mu_s (1 - \phi) d_s - \mu_f \phi d_s S} \qquad (A.2)$$

where

S is fluid saturation,
d represents thickness,
μ represents attenuation coefficient

and subscript

w refers to the wall material
s refers to the soil sample,
f refers to the fluid.

This equation may be solved for S if all other variables are known.

Values for μ_w, μ_s, μ_f were obtained directly by use of test samples. A test stand was constructed in which the source and detector were held in the same relative positions as when mounted on the flume. The source used was 100 millicuries of Americium, with collimation to a 3/16" diameter beam. A sample container made of plexiglass, whose walls duplicated the soil flume in thickness and spacing, was placed between the source and detector, and μ_w was calculated by the attenuation with the box empty. Using this same container filler with the fluid provided a means to calculate μ_f. Similarly, filling the container with dry soil at a known porosity, and taking attenuation measurements at several different points through the sample section allowed calculation of μ_s as follows:

$$\text{Use} \quad \bar{I} = I_o e^{-\mu_s (1 - \phi) d_s - \mu_s d_w} \quad ,$$

solving for μ_s,

$$\mu_s = \frac{-\ln \left[I / I_o \right] \mu_w d_w}{(1 - \phi) d_s} \quad . \qquad (A.3)$$

For computations at selected points on the flume, it was necessary to determine the local value of $\phi(x,z)$. This was accomplished by saturating the flume, taking attenuation readings, and then solving equation (A.2) for ϕ. Some error was introduced here because at many points S was less than 1.0, due to air trapped during imbibition.

With the necessary attenuation coefficients and other constants thus determined, equation (A.2) may be solved for S:

$$S = \frac{\ln(I_o/I) - \mu_w d_w - \mu_s d_s (1 - \phi)}{\phi \mu_f d_s} \quad . \qquad (A.4)$$

From such computations with experimental data, some inferences could be made regarding the sensitivity of the computed S to errors in parameters in equation (A.4). The most sensitive parameter appears to be d_s, followed in an uncertain order by I, μ_s, and I_o. It is assumed that μ_f and μ_w were well determined by the sample test procedure.

For the experiments described in this paper, slight mechanical play and eccentric weighting of the support racks caused small variations in relative orientation of the γ-source and detector. Thus I_o was a function of vertical position relative to the top of the flume. Similarly, d_s was slightly variable along the vertical section due to soil pressure bulging. These variations were determined and applied in the solution of equation (A.4).

From laboratory experience and calculations with data collected, it is estimated that measured saturations are reliable within $\pm$ 10%. This figure could be improved markedly by use of better counting equipment which is currently available, and a better designed flume arrangement.

Key Words: Infiltration, overland flow, unsaturated flow in porous media, kinematic wave, finite-difference methods.

Abstract: The partial differential equation for vertical, one-phase, unsaturated flow of water in soils is used as a mathematical model governing infiltration. A nonlinear Crank-Nicolson implicit finite-difference scheme is used to obtain solutions to this equation for realistic initial and upper boundary conditions. The kinematic wave approximation to the equations of unsteady overland flow on cascaded planes is used for the mathematical model of surface runoff. The difference equations of infiltration and overland flow are combined into a model for a simple watershed, employing computational logic so that boundary conditions match at the soil surface. The mathematical model is tested by comparison with data from a laboratory soil flume and with data from a small experimental watershed.

Reference: Roger E. Smith and David A. Woolhiser, Colorado State University Hydrology Paper No. 47 (January 1971) "Mathematical Simulation of Infiltrating Watersheds."

Key Words: Infiltration, overland flow, unsaturated flow in porous media, kinematic wave, finite-difference methods.

Abstract: The partial differential equation for vertical, one-phase, unsaturated flow of water in soils is used as a mathematical model governing infiltration. A nonlinear Crank-Nicolson implicit finite-difference scheme is used to obtain solutions to this equation for realistic initial and upper boundary conditions. The kinematic wave approximation to the equations of unsteady overland flow on cascaded planes is used for the mathematical model of surface runoff. The difference equations of infiltration and overland flow are combined into a model for a simple watershed, employing computational logic so that boundary conditions match at the soil surface. The mathematical model is tested by comparison with data from a laboratory soil flume and with data from a small experimental watershed.

Reference: Roger E. Smith and David A. Woolhiser, Colorado State University Hydrology Paper No. 47 (January 1971) "Mathematical Simulation of Infiltrating Watersheds."

Key Words: Infiltration, overland flow, unsaturated flow in porous media, kinematic wave, finite-difference methods.

Abstract: The partial differential equation for vertical, one-phase, unsaturated flow of water in soils is used as a mathematical model governing infiltration. A nonlinear Crank-Nicolson implicit finite-difference scheme is used to obtain solutions to this equation for realistic initial and upper boundary conditions. The kinematic wave approximation to the equations of unsteady overland flow on cascaded planes is used for the mathematical model of surface runoff. The difference equations of infiltration and overland flow are combined into a model for a simple watershed, employing computational logic so that boundary conditions match at the soil surface. The mathematical model is tested by comparison with data from a laboratory soil flume and with data from a small experimental watershed.

Reference: Roger E. Smith and David A. Woolhiser, Colorado State University Hydrology Paper No. 47 (January 1971) "Mathematical Simulation of Infiltrating Watersheds."

Key Words: Infiltration, overland flow, unsaturated flow in porous media, kinematic wave, finite-difference methods.

Abstract: The partial differential equation for vertical, one-phase, unsaturated flow of water in soils is used as a mathematical model governing infiltration. A nonlinear Crank-Nicolson implicit finite-difference scheme is used to obtain solutions to this equation for realistic initial and upper boundary conditions. The kinematic wave approximation to the equations of unsteady overland flow on cascaded planes is used for the mathematical model of surface runoff. The difference equations of infiltration and overland flow are combined into a model for a simple watershed, employing computational logic so that boundary conditions match at the soil surface. The mathematical model is tested by comparison with data from a laboratory soil flume and with data from a small experimental watershed.

Reference: Roger E. Smith and David A. Woolhiser, Colorado State University Hydrology Paper No. 47 (January 1971) "Mathematical Simulation of Infiltrating Watersheds."

PREVIOUSLY PUBLISHED PAPERS

Colorado State University Hydrology Papers

No. 31 "Effects of Truncation on Dependence in Hydrologic Time Series," by Rezaul Karim Bhuiya and Vujica Yevjevich, November 1968.

No. 32 "Properties of Non-Homogeneous Hydrologic Series," by V. Yevjevich and R. I.Jeng, April 1969.

No. 33 "Runs of Precipitation Series," by Jose Llamas and M. M. Siddiqui, May 1969.

No. 34 "Statistical Discrimination of Change in Daily Runoff," by Andre J. Dumas and Hubert J. Morel-Seytoux, August 1969.

No. 35 "Stochastic Process of Precipitation," by P. Todorovic and V. Yevjevich, September 1969.

No. 36 "Suitability of the Upper Colorado River Basin for Precipitation Management," by Hiroshi Nakamichi and Hubert J. Morel-Seytoux, October 1969.

No. 37 "Regional Discrimination of Change in Runoff," by Viboon Nimmannit and Hubert J. Morel-Seytoux, November 1969.

No. 38 "Evaluation of the Effect of Impoundment on Water Quality in Cheney Reservoir," by J. C. Ward and S. Karaki, March 1970.

No. 39 "The Kinematic Cascade as a Hydrologic Model," by David F. Kibler and David A. Woolhiser, February 1970.

No. 40 "Application of Run-Lengths to Hydrologic Series," by Jaime Saldarriaga and Vujica Yevjevich, April 1970.

No. 41 "Numerical Simulation of Dispersion in Groundwater Aquivers," by Donald Lee Reddell and Daniel K. Sunada, June 1970.

No. 42 "Theoretical Probability Distributions for Flood Peaks," by Emir Zelenhasic, November 1970.

No. 43 "Flood Routing Through Storm Drains, Part I, Solution of Problems of Unsteady Free Surface Flow in a Storm Drain," by V. Yevjevich and A. H. Barnes, November 1970.

No. 44 "Flood Routing Through Storm Drains, Part II, Physical Facilities and Experiments," by V. Yevjevich and A. H. Barnes, November 1970.

No. 45 "Flood Routing Through Storm Drains, Part III, Evaluation of Geometric and Hydraulic Parameters," by V. Yevjevich and A. H. Barnes, November 1970.

No. 46 "Flood Routing Through Storm Drains, Part IV, Numerical Computer Methods of Solution," by V. Yevjevich and A. H. Barnes, November 1970.